

The First *Insight-HXMT* Gamma-Ray Burst Catalog: The First Four Years

XIN-YING SONG,¹ SHAO-LIN XIONG,¹ SHUANG-NAN ZHANG,^{1,2} CHENG-KUI LI,¹ XIAO-BO LI,¹ YUE HUANG,¹ CRISTIANO GUIDORZI,^{3,4,5} FILIPPO FRONTERA,^{3,5} CONG-ZHAN LIU,¹ XU-FANG LI,¹ GANG LI,¹ JIN-YUAN LIAO,¹ CE CAI,^{1,2} QI LUO,^{1,2} SHUO XIAO,^{1,2} QI-BIN YI,^{1,6} YAO-GUANG ZHENG,^{1,7} DENG-KE ZHOU,^{1,2} JIA-CONG LIU,^{1,2} WANG-CHEN XUE,^{1,2} YAN-QIU ZHANG,^{1,2} CHAO ZHENG,^{1,2} ZHI CHANG,¹ ZHENG-WEI LI,¹ XUE-FENG LU,¹ AI-MEI ZHANG,¹ YI-FEI ZHANG,¹ YONG-JIE JIN,⁸ TI-PEI LI,^{1,8} FANG-JUN LU,^{1,2} LI-MING SONG,^{1,2} MEI WU,¹ YU-PENG XU,¹ XIANG MA,¹ MING-YU GE,¹ SHU-MEI JIA,¹ BING LI,¹ JIAN-YIN NIE,¹ LING-JUN WANG,¹ JUAN ZHANG,¹ SHI-JIE ZHENG,¹ XUE-JUAN YANG,⁶ AND RONG-JIA YANG⁷

¹Key Laboratory of Particle Astrophysics, Institute of High Energy Physics, Chinese Academy of Sciences, Beijing 100049, China

²University of Chinese Academy of Sciences, Chinese Academy of Sciences, Beijing 100049, China

³Department of Physics and Earth Science, University of Ferrara, Via Saragat 1, I-44122 Ferrara, Italy

⁴INFN - Sezione di Ferrara, Via Saragat 1, I-44122 Ferrara, Italy

⁵INAF - Osservatorio di Astrofisica e Scienza dello Spazio di Bologna, Via Piero Gobetti 101, I-40129 Bologna, Italy

⁶Department of Physics, Xiangtan University, Xiangtan, Hunan Province 411105, China

⁷College of physics Sciences & Technology, Hebei University, No. 180 Wusi Dong Road, Lian Chi District, Baoding City, Hebei Province 071002, China

⁸Department of Engineering Physics, Tsinghua University, Beijing 100084, China

ABSTRACT

The Hard X-ray Modulation Telescope (*Insight-HXMT*), is China’s first X-ray astronomy satellite launched on June 15, 2017. The anti-coincidence CsI detectors of the High Energy X-ray telescope (HE) onboard *Insight-HXMT* could serve as an all-sky gamma-ray monitor in about 0.2-3 MeV. In its first four years of operation, *Insight-HXMT* has detected 322 Gamma-Ray Bursts (GRBs) by offline search pipeline including blind search and targeted search. For the GOLDEN sample of *Insight-HXMT* GRBs, joint analyses were performed with other GRB missions, including *Fermi* Gamma-ray Burst Monitor (*Fermi*/GBM), Swift Burst Alert Telescope (*Swift*/BAT) and Gravitational wave high-energy Electromagnetic Counterpart All-sky Monitor (GECAM). It shows that *Insight-HXMT* can provide better constraint on GRB spectrum at higher energy band. The properties of *Insight-HXMT* GRBs are reported in detail, including their trigger time, duration, spectral parameters, peak fluxes of different time scales and fluence. This catalog is an official product of the *Insight-HXMT* GRB team.

Keywords: catalogs – gamma-ray burst: general

1. INTRODUCTION

The Hard X-ray Modulation Telescope (HXMT), dubbed *Insight-HXMT*, launched on June 15, 2017, is China’s first X-ray astronomy satellite devoted to broad band observations in the 1-250 keV band. *Insight-HXMT* consists of three collimator-based telescopes: the High Energy X-ray Telescope (HE, Liu et al. 2020), the Medium Energy X-ray Telescope (ME, Cao et al. 2020) and the Low Energy X-ray Telescope (LE, Chen et al. 2020). *Insight-HXMT*/HE adopts an array of 18 NaI(Tl)/CsI(Na) phoswich detectors as the main detec-

tor plane, with a total geometric area of about 5100 cm² and a combined Field of View (FOV) of about 5.7°×5.7° (FWHM)(HE, Liu et al. 2020). The CsI(Na) (CsI for brevity) in the phoswich detector of HE can be also used as an all-sky gamma-ray monitor in 0.2-3 MeV, since gamma-rays in this energy range can penetrate the spacecraft and deposit energy in the CsI detector. Thus HE could play an important role in monitoring gamma-ray bursts (GRBs), MeV pulsars, Solar Flares (SFL), Terrestrial Gamma-ray Flashes (TGF) and other gamma-ray sources. The measured energy range (deposited energy) of CsI is about 40-800 keV in the normal gain (NG) mode and about 200 keV- 3 MeV in low gain (LG) mode. The NG and LG modes are achieved by

Corresponding author: Shao-Lin Xiong, Shuang-Nan Zhang
 xiongsl@ihep.ac.cn, zhangsn@ihep.ac.cn

adjusting the high voltage of the PMTs which readout the NaI(Tl)/CsI(Na) phoswich detectors.

There is neither on-board GRB trigger system nor prompt data telemetry for *Insight*-HXMT, thus GRBs are unveiled on-ground using two pipelines: the blind search is performed on all data acquired by *Insight*-HXMT/HE CsI detector; in addition, for each GRB detected by other astronomical satellites or instruments (called external triggers hereafter, in contrast to the internal triggers produced by *Insight*-HXMT itself) reported through the Gamma-ray Coordinates Network (GCN), the targeted search pipeline would be launched to search CsI data around the trigger time of external triggers.

From June 26th in 2017 to June 30th 2021, GRBs and others bursts including terrestrial gamma-ray flash (TGF), solar flares (SFL, Zhang et al. 2021) have been detected by *Insight*-HXMT, the gamma-ray counterparts of Gravitational Wave (GW) events (Li et al. 2018a; Zhang et al. 2018; Li et al. 2017); Fast radio bursts (FRB, Guidorzi et al. 2020)) and High Energy Neutrino (HEN, e.g. Zheng et al. 2020), have been monitored as well. During the first four years of observation data, 660 bursts are found, where 322 are classified as GRBs, 245 as TGFs, 4 as SFLs, 33 as charged particles and 56 as unclassified. Targeted search were implemented for external triggers of great importance, including 41 HENs, 48 GWs and 39 FRBs. For each GRB, the trigger time in Universal Time Coordinated (UTC) and Mission Elapsed Time (MET) are recorded and the event data is selected between $T_0 - 100\text{s}$ and $T_0 + 300\text{s}$ in most cases, where T_0 is trigger time from GCN or blind search. In addition, quick-analysis tools for GRBs and joint spectral fitting with other missions are developed for this catalog analysis, which are introduced in the following sections.

We start with a brief description of the HXMT/CsI detectors and calibration in Section 2 and refer Luo et al. (2020) for a more thorough and complete description of the instrument and calibration respectively. This is followed, in Section 3 the burst-searching algorithm and its up-to-date ability is introduced in details. In Section 4, a description of the methodology used in the production of this catalog is presented, including detector selection, data types used, energy selection and background fitting, and the source selection. In Section 5, catalog analysis and results are presented. In Section 6, the distribution of duration, hardness are discussed and all the GRBs catalog results are summarized.

2. INSTRUMENT

The High Energy X-ray Telescope (HE, Liu et al. 2020) consists of the main detector (HED), high energy collimator (HEC), auto-gain control detector (HGC), anti-coincidence shield detector (HVT), particle monitor (HPM), data processing and control box (HEB) and power box (HEA). As the main detector of HE, HED is responsible for the observation of celestial sources. It consists of 18 NaI(Tl)/CsI(Na) phoswich detectors (labelled as HED-0, 1 ... to 17), each with a diameter of 190 mm and a collimator made of lead and tantalum. The NaI detectors are sensitive to the hard X-rays in 20-250 keV, whereas the CsI acts as an anti-coincidence detector to reduce the background of NaI. The thickness of the NaI and CsI crystals are 3.5 mm and 40 mm, respectively. HGC provides the auto-gain control and energy calibration for HED. HVTs act as an active shielding system to reduce HED's background caused by charged particles. HPMs monitor the flux of charged particles and send out an alert to switch off the high voltages of HEDs and HVTs in high flux regions to avoid potential damage to the PMTs of these detectors. The overview of all telescopes aboard *Insight*-HXMT is shown in Figure 1.

Insight-HXMT/HE can observe the high energy sky with two observation scenarios (Zhang et al. 2020) which can work simultaneously:

- (1) Collimator-based (pointed or scan) observation: using NaI/CsI detectors, HE can detect hard X-ray emission in 20-250 keV from the celestial sources within the FOV defined by collimators. HE can do pointed observation to a specific source, or scan observation to a small sky area.
- (2) Gamma-ray all-sky monitoring: Gamma-ray photons with energy higher than ~ 200 keV from all directions can penetrate the spacecraft and be detected by the CsI detectors. CsI can monitor the gamma-ray all-sky with the only exception of the occulted region by the Earth. This gamma-ray all-sky monitoring is an extended capability for HE and inapplicable for ME or LE telescopes aboard *Insight*-HXMT.

The primary observation scenario of HE is the collimator-based observation consisting of pointed observation and scan observation, both of which use the NaI as the main detector and detect sources within the field of view (FOV) of collimator in 20-250 keV. The CsI detectors mainly act as the anti-coincidence and shielding to reduce the background of NaI. Due to the high thickness of the CsI(Na) crystals, high energy (greater than about 200 keV) gamma-ray photons can penetrate the spacecraft and be recorded by the CsI

detectors, thus the GRBs unocculted by the Earth can be detected. For each NaI/CsI phoswich detector of HE, the event-by-event data (called EVT data hereafter) is recorded and we can use the pulse width information in the EVT data to distinguish between NaI events and CsI events. For this paper, we only select these events recorded by CsI detectors by screening events with pulse width greater than 75. The response and calibration of the CsI detectors are mainly described in Section 4.1.

The gain of NaI/CsI detector is mainly controlled by the High Voltage of the PMT which converts the scintillation light produced by NaI/CsI crystals to the electric signals. To meet various observation requirements, two gain modes are designed for the HE NaI/CsI detectors: normal gain (NG) mode and low gain (LG) mode. The measured energy ranges for CsI detector are listed as below: the NG mode in 40–800 keV and the LG mode in 200–3000 keV (both refer to the deposited energies). NG mode is the main working mode that the auto-gain control system can keep the full-energy-peak of the 59.5 keV photons (emitted from a radioactive source ^{241}Am) in a fixed channel of the NaI detector. In LG mode, the high voltage of the each *Insight-HXMT*/HE detector is reduced and the auto-gain control system is disabled to achieve a higher energy range detection. As derived from the two-year observations since *Insight-HXMT* has operated in-orbit, the E-C relationships of each *Insight-HXMT*/CsI detector for both NG and LG modes vary over time, so calibration of the instrumental response is of great importance.

3. SEARCH FOR BURSTS

A pipeline is developed to search for GRBs for blind search and the coherent search method for targeted search (Cai et al. 2021). The blind search software continually monitors each group (18 CsI detectors are divided into 6 groups, 3 in each group) of detectors count rates, for which the reason is to reduce statistical fluctuations of one or a few detectors, one of the main causes of false trigger. The pipeline is triggered when counts rates in the EVT data of three or more groups of CsI detectors exceed the background counts rates, by 3σ on five timescales: 0.05s, 0.1s, 0.2s, 0.5s and 1s by calculating an average of the counts rates of 10 s of the previous data as background.

If a GRB detected by other external missions, falls in the field of view of HE, but did not trigger the blind search, targeted search in HE/CsI data would be launched. The targeted coherent search method is applied to the EVT data of HE CsI detectors, which can recover true astrophysical bursts that are too weak to trigger through blind search. This coherent method

was originally developed by Blackburn et al. (2015), improved by Goldstein et al. (2016), Goldstein et al. (2019), and verified by Kocevski et al. (2018). From the statistics of searched GRBs, we find the fluence (from GBM Burst Catalog) of HE targeted search could reach $\sim 10^{-7}$ erg cm $^{-2}$ (10 keV–1 MeV) in duration of 0.256 s. For this paper, 15 GRBs that are found from targeted search are included and labeled in Table 3, while the rest are from blind search. Details of burst search are presented in a separate paper (Cai et al. 2021).

4. CATALOG ANALYSIS

4.1. Instrument Response

There are two parts in the instrumental response of CsI detectors: the energy redistribution of the photons from incident energy to deposition energy that is determined by the property of the CsI crystal and the mass distribution of satellite; and the Energy-Channel (E-C) relationship that is determined by the detectors and electronic system of the instrument. For the photon energy redistribution, the reliability is mainly determined by the accuracy of the mass model of the satellite and the payloads (Agostinelli et al. 2003). Based on the initial mass model of the satellite platform (Xie et al. 2015), we calibrate the mass model with the Crab pulse radiation as a standard candle (Li et al. 2018b), to generate accurate instrumental response for the all sky gamma-ray monitoring.

The in-flight E-C relationship and energy resolution of the instrument can be obtained by analyzing the characteristic lines of the in-orbit observed and the on-ground simulated background spectra (Li et al. 2019). The E-C relationship varies over time, whereas the energy resolution remains stable (Li et al. 2020). Therefore, we update the E-C relationship every month, and take the average energy resolution of all calibration results to generate the instrumental response.

After the above calibration, a new response matrix library is established and a simulated spectral analysis is performed to test the HXMT/CsI spectroscopy capabilities. Calibration of the instrumental response to GRB is carried out with GRBs (Luo et al. 2020). In a GRB observation, the incident direction of the GRB photons is supposed to be arbitrary, however, only the instrumental response to several directions can be calibrated directly. A common method of the instrumental response testing is the cross-calibration with other instruments by comparing the energy spectrum of the simultaneously observed GRB (Sakamoto et al. 2011; Tsujimoto et al. 2011; Tierney et al. 2010; Ishida et al. 2014). The detection efficiency of HXMT/CsI is checked by the joint spectral analyses with *Fermi*/GBM, *Swift*/BAT

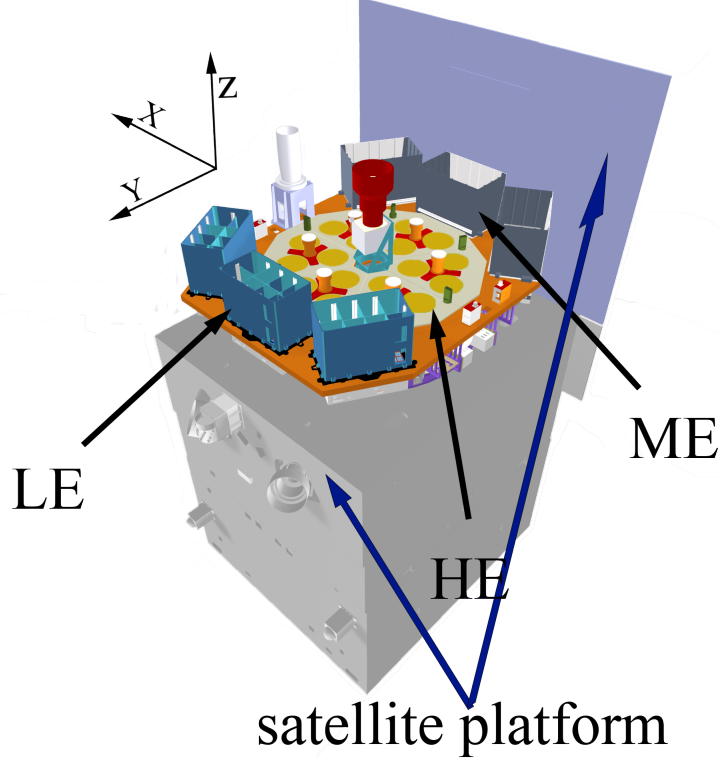


Figure 1. The illustration of the satellite platform and the payloads of *Insight-HXMT*. The coordinate system used in this study is shown on the upper-left. It is adapted from Fig. 1 in [Luo et al. \(2020\)](#).

and *Konus-Wind*, in which we find that HXMT/CsI can provide better constraint on GRB spectrum at higher energy band ([Luo et al. 2020](#)). The instrumental responses are mainly obtained by Monte Carlo simulation with the Geant4 tool and the mass model of both the satellite and all the payloads, which is updated and tested with the Crab pulse emission in various incident directions. Both the Energy-Channel relationship and the energy resolution are calibrated in two working modes (NG mode and LG mode) with the different detection energy ranges. The simulated spectral analyses show that HXMT/CsI can constrain the spectral parameters much better in the high energy band than that in the low energy band. As introduced in ([Luo et al. 2020](#)), the joint spectral analyses are performed to ten bright GRBs observed simultaneously with HXMT/CsI and other instruments (*Fermi*/GBM, *Swift*/BAT, *Konus-Wind*), and the results show that the GRB flux given by HXMT/CsI is systematically higher by $7.0 \pm 8.8\%$ than those given by the other instruments. The HXMT/CsI-*Fermi*/GBM joint fittings also show that the high energy spectral parameter can be constrained much better as the HXMT/CsI data are used in the joint fittings.

In summary, the instrumental responses of the HXMT/CsI detectors of *Insight-HXMT* are well cali-

brated in aspects of mass model, E-C relationship and the energy resolutions for both the NG and LG modes. Thanks to the large effective area in the high-energy band, as shown in Figure 2, HXMT/CsI shows its advantages in constraining the GRB spectra in high energy band, together with other missions (such as *Fermi*/GBM) which provide observations at lower energies.

Note that the deposited energy range is usually very different from incident energy bands due to the responses of HXMT/CsI detectors. Three types of spectra are listed in Table 1, where the soft and middle spectra are with BAND model, the hard spectra is with CPL model, and they are representative of GRBs of different hardness; details of BAND and CPL model are clarified in Section 4.7.1. They are simulated with the same amplitude in each type of spectra (use *fakeit* in Xspec 12.11.0, with all the model normalization factors equal to 1), and convoluted with the total response of 18 HXMT/CsI detectors. The deposited energy spectra of incident angle theta from 0° to 180° are shown in NG mode (Figure 3) and in LG mode (Figure 4) respectively, which shows the ranges of deposited energy. Considering the deposited spectra and effective area shown in Figure 2, the deposited energy range of HXMT/CsI data

Comparision of effective areas of different missions

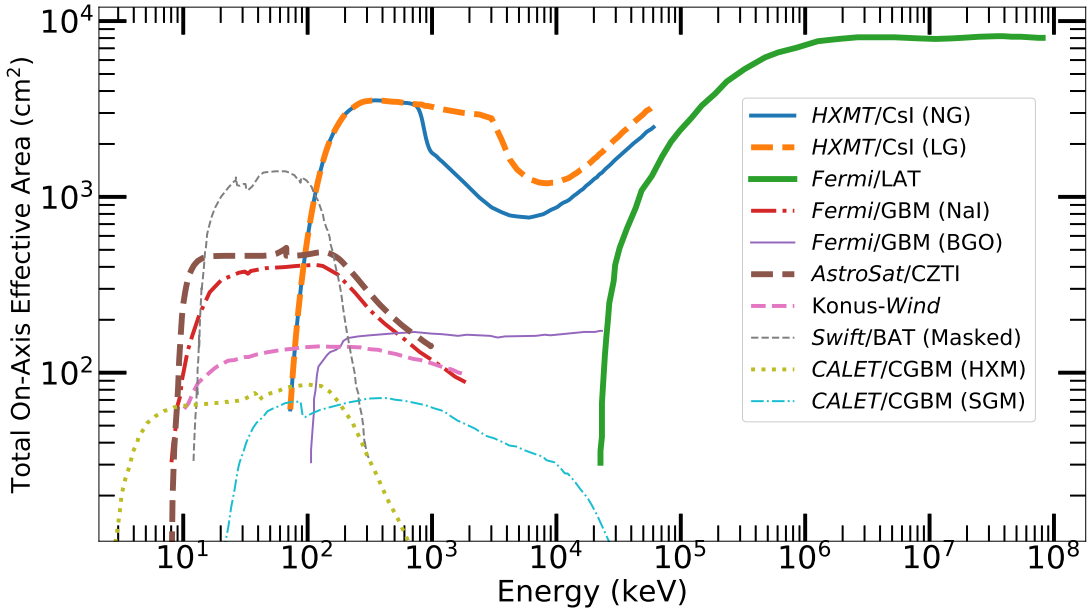


Figure 2. Effective areas of HXMT/CsI, *Fermi*/LAT, *Fermi*/GBM, Konus-Wind, *Swift*/BAT, CALET/CGBM and *AstroSat*/CZTI. The effective area of *Fermi*/GBM (NaI) is the averaged over the unocculted sky. It is adapted from Fig. 13 in Luo et al. (2020).

Table 1. Three types of spectra and parameters. The soft and middle spectra are with BAND model, and the hard spectra is with CPL model.

Types of spectra	α	β	$E_{\text{peak}}(\text{keV})$
SOFT	-1.9	-3.7	70
MIDDLE	-1.0	-2.0	230
HARD	-0.5	-	1500

is determined to be about 150-800 keV for NG mode and about 200-3000 keV for LG mode in the following spectra analysis.

4.2. GRB Samples

In summary, we define three types of GRB samples as shown in Table 2. Only the ‘GOLDEN’ GRBs could be utilized in the joint analysis, which are required to be located well and detected without saturation in HXMT/CsI data. The ‘SILVER’ samples denote those which are detected by other external missions, but not located or lack of data for joint analysis. In this analysis, public data offered by *Fermi*/GBM, *Swift*/BAT or GECAM are utilized for joint analysis. The bursts which are only detected by HXMT are labeled as ‘BRONZE’. **The HXMT/HE data files will not be used if there is saturation in electronics subsystem during the GRBs, or the data quality is not good (such as data loss).** Saturation is defined when

the two following criteria are matched simultaneously: firstly, total count rate of 18 CsI detectors exceeds 20000 counts/s, as evaluated over four different timescales: 0.1, 0.2, 0.5, and 1.0 s; secondly, in at least one of the three groups of 6 CsI detectors that share the same Analog-to-Digital Converter (ADC) (Liu et al. 2020), the total light curve has at least one 5-ms bin with zero counts. As shown in Table 2, this kind of GRB samples are labeled as ‘IRON’, which are not utilized in the following analysis.

4.3. Suppression of Background From Charged Particles

Among the main detectors of the HE telescope, HVTs act as an active shielding system to reduce HED background caused by charged particles (HE, Liu et al. 2020). In order to suppress the background from charged particles, events which are coincidence with signal in HVTs are removed since they are likely produced by charged particles rather than gamma-rays. Besides, those events which also have energy deposition in NaI (Tl) detectors are also eliminated, because the signals of NaI (Tl) are mainly from the target source when we perform pointed or scan observation. Response of 18 CsI detectors in HED according to Section 2 are different but the discrepancy between them are small (unlike the case

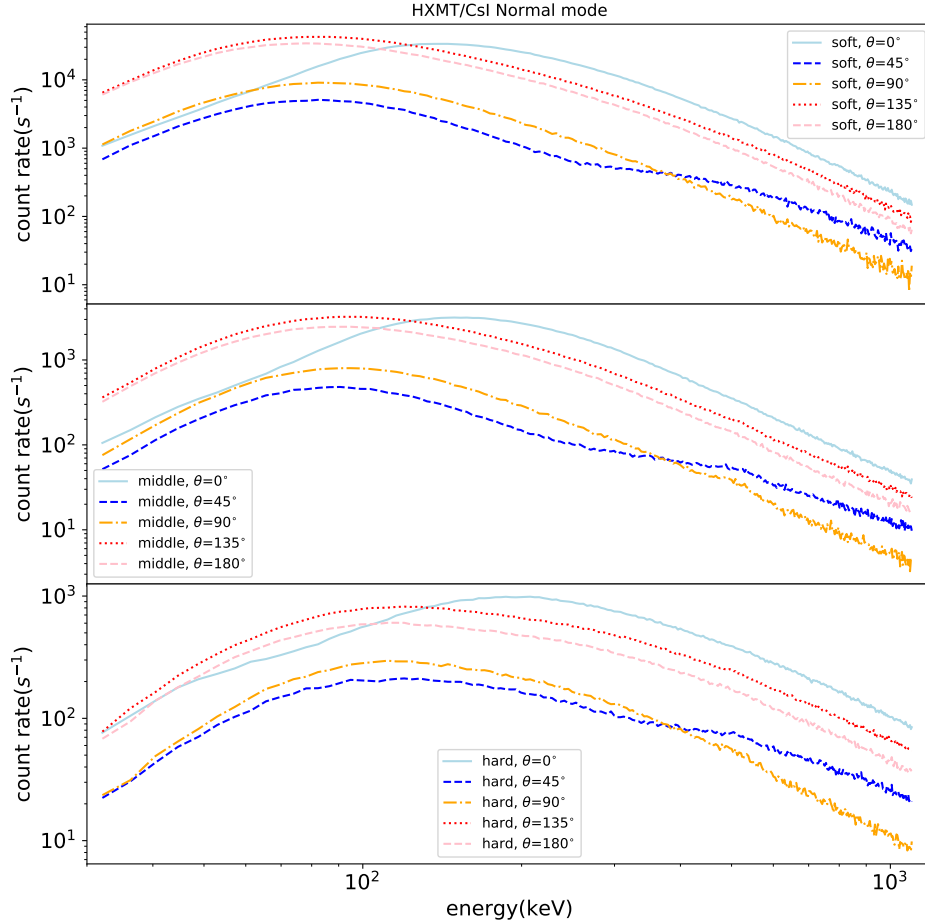


Figure 3. The deposited energy spectra of three types of BAND with incident angle θ of 0° to 180° are shown in NG mode. The azimuthal angle ϕ is 0° . Here the incident angle θ and the azimuthal angle ϕ denote the direction of gamma rays in spherical coordinates of HE/CsI detector.

Table 2. Classification of four kinds of *Insight-HXMT* GRB samples.

Type	Location and data for joint analysis	External detected	Saturation in HXMT data	Utilized or not	Number
GOLDEN	Yes	Yes	No	Yes	202
SILVER	No	Yes	No	No	44
BRONZE	No	No	No	No	50
IRON	Yes/No	Yes/No	Yes	No	26

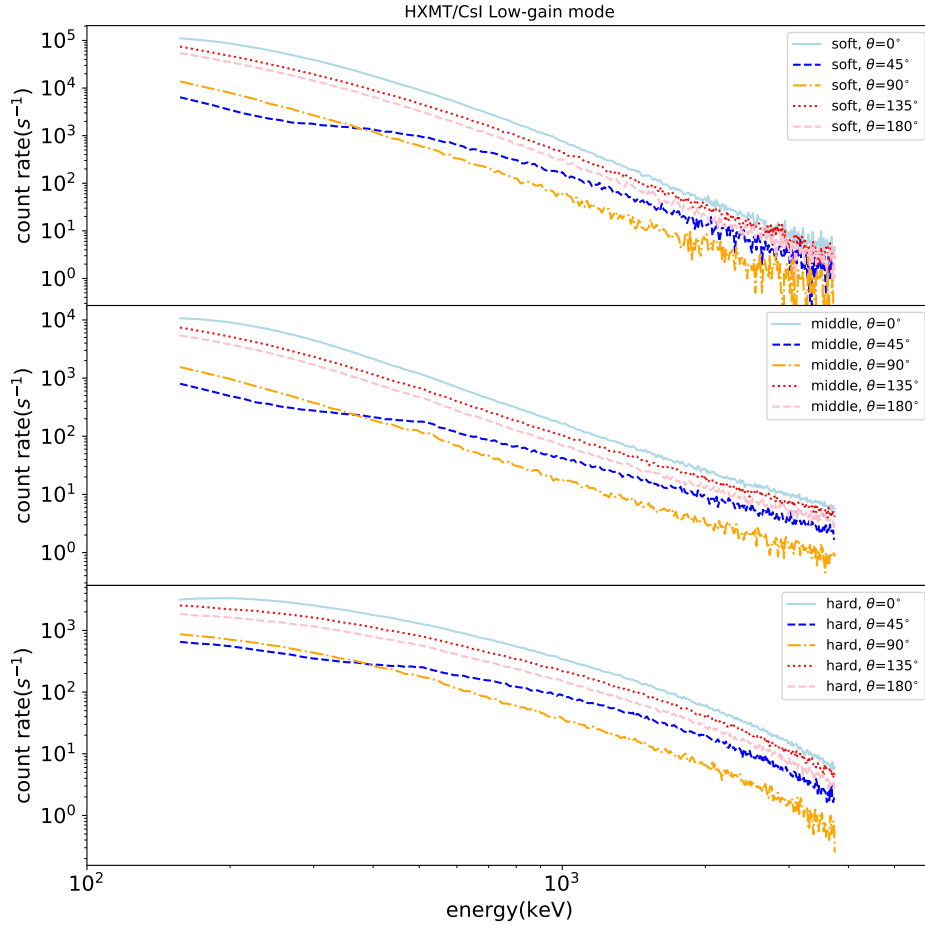


Figure 4. The deposited energy spectra of three types of BAND with incident angle θ of 0° to 180° are shown in LG mode. The azimuthal angle ϕ is 0°. Here the incident angle θ and the azimuthal angle ϕ denote the direction of gamma rays in spherical coordinates of HE/CsI detector.

in *Fermi*/GBM or GECAM where detectors have different orientations), therefore, all dat events in 18 CsI detectors are utilized in this study.

4.4. Dead Time Correction

Dead time of HED detectors is complicated. According to Xiao et al. (2020), every 6 detectors in 18 NaI (Tl)/CsI (Na) detectors in HE share one ADC read-out electronics, thus a signal in any detector will cause dead time not only to the incident detector itself, but also to the other 5 detectors of the same ADC. The dead time of one event is normally about $4 \sim 8 \mu\text{s}$, but it will be longer for the signals generated by high energy charged particles. There is a dead time counter in HEB for each HED, and the information is recorded in the form of proportion of dead time. The proportion of dead time in a time interval is determined with the method established in Xiao et al. (2020). The correction factors on the light curves are determined by $\frac{1}{1-P_{\text{dt}}}$, where P_{dt} is the proportion of dead time in every time bin with bin width of 10 ms. The light curves of each CsI detector are corrected by multiplying with series of dead-time correction factors before background fitting is performed. As shown in Figure 5, the comparison between light curves with and without dead-time correction of a short GRB is present, which shows that the dead-time correction is necessary for refined analysis.

4.5. Background Fitting

After the data have been selected for a given GRB, a background model in the form of polynomial function with time, is computed separately for each detector, based on user-selected time intervals for background region. Here we use a pre-burst interval and a post-burst interval as user-selected background regions. The order of polynomial is determined by the best goodness of fits with polynomials of different orders, where the order could be 0, 1, 2 respectively. For each detector, background fitting is carried out for each energy channel, and the background fit determined from pre-burst and post-burst intervals are used to estimate the background counts in the signal region of the burst. The net counts number of GRB in each channel is obtained by subtracting the counts of background from the total counts number. Background fitting is performed in each detector channel by channel in deposited energy spectrum, until the net counts and background counts of all channels for the given GRB are determined. Statistical errors of net counts are determined by the root of the sum of squares of the statistical errors of background estimation and Poisson errors of total counts (i.e. classical error propagation). Note that all light curves

for each energy channel in each detector have been corrected with dead-time correction factors. The source time intervals for all detectors are chosen to be same for the GRB data analysis, thus data of all detectors could be added up to reduce the statistical uncertainties.

4.6. Source Time Interval Selection

Source time interval selection may be different when we perform different analyses. For the computation of duration, peak fluxes and fluence, the source interval is loosely selected, by starting from several seconds before the burst begins and ending at several seconds after the burst ends, and may have overlaps with pre-burst and post-burst intervals for background selection. If there exists difference of start- and end-time of a GRB between HXMT/CsI and other missions due to the energy detection range, the loosest source interval is applied for the joint data analysis of these missions. For the analysis of time-average spectra, the source time interval is usually selected to be narrower. The events in T_{90} or the whole duration in some cases based on deposited photon counts are selected for the time-averaged energy spectra.

In the case of joint analyses with other missions, the time delay due to the different arrival times of two space-crafts is considered. The method mentioned in Hurley et al. (1999) is utilized to determine the time delay between HXMT and other missions. Figure 6 shows the time delays of other missions relative to HXMT for ‘GOLDEN’ GRB samples. The red histograms denote the time delays of *Fermi*/GBM, while the blue ones denote those of *Swift*/BAT and the green ones for those of GECAM. The negative values represent that GRBs arrived at other missions earlier than HXMT, while the positive numbers means that the GRB arrival time of HXMT is earlier. Some time delays reach up to tens of milliseconds and must be considered, because the time scale (64 ms) of deconvolved photon spectra is in the same order of magnitude.

4.7. Duration, Fluence and Peak Flux

In order to take advantages of different missions and to reduce uncertainties in determination of the parameters of GRBs, joint spectral analyses between HXMT and *Fermi*/GBM, *Swift*/BAT and GECAM are applied on all ‘GOLDEN’ GRBs. This paper reports various measures of the duration, peak fluxes and fluence of each burst. We take **GRB 200125B (HEB200125863)**, **GRB 210121A (HEB2101210779)** and **GRB 210112A (HEB210112068)** as samples to show the procedures performed on all GRBs in Appendix A. The fits to time-averaged and time-resolved spectra are all performed with Xspec 12.11.0.

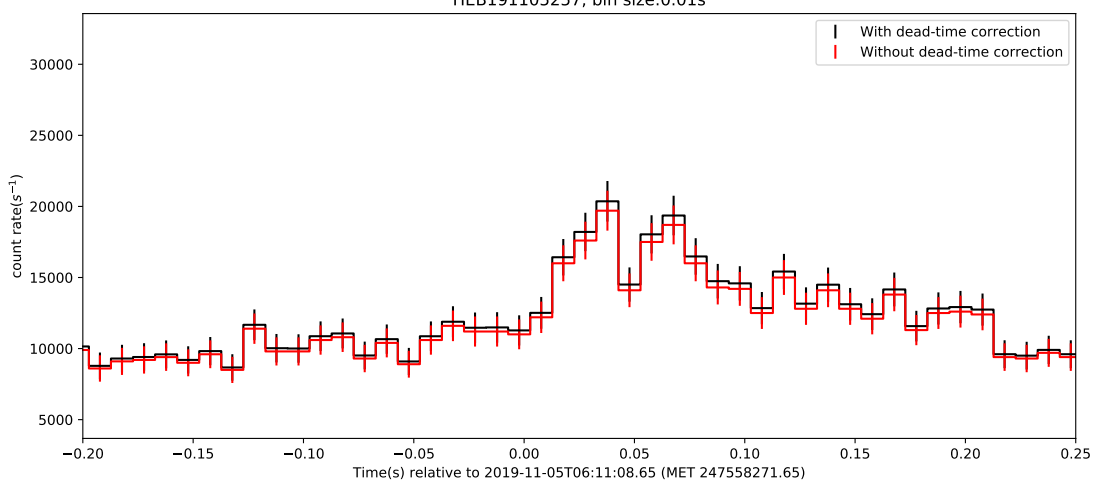


Figure 5. A comparison between light curves with and without dead-time correction of a short GRB triggered at 2019-11-05T06:11:08.65 UTC. The histogram of red lines and error bars denote the light curve without dead-time correction, while the black with dead-time correction. Here MET means the mission elapsed time of HXMT.

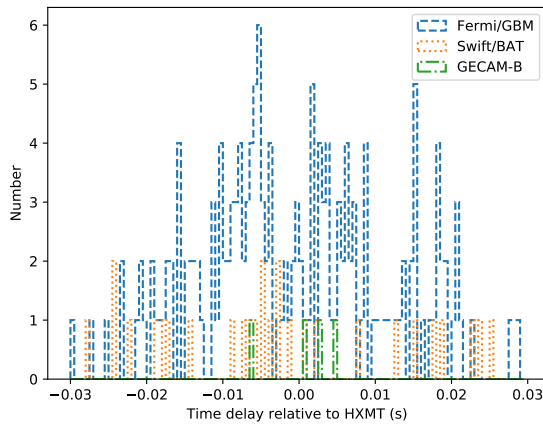


Figure 6. The distribution from ‘GOLDEN’ GRB samples of time delays of *Fermi*/GBM (dashed), *Swift*/BAT (dotted), and GECAM (dot-dashed) relative to HXMT are shown.

4.7.1. Time-Average Spectrum

The time-averaged energy spectra are obtained from HXMT/CsI together with other instruments. For example, from *Fermi*/GBM, the spectra from two NaI(Tl) scintillation detectors working at 8 keV – 1 MeV and one BGO scintillation detectors at \sim 200 keV to \sim 4 MeV are selected according to the statistics of GRB signal. A joint fit with time-averaged energy spectra from HXMT/CsI and three (two NaI and one BGO) spectra from *Fermi*/GBM are performed, where the parameters of GRB spectral shape are shared but the amplitudes are set to be float for these four sets of data, to compensate the possible lack information either in the

adopted spectrum model or the understanding of the instruments response. In most cases, the amplitudes of fitted spectra are consistent well with each other within one standard deviation.

To perform the joint fit, 6 models are chosen including a single power law (PL), Band’s GRB function (BAND, Band et al. (1993)), an exponential cut-off power law (CPL, also called Comptonized Model) and plus a component of black body function (BB) of float amplitudes. The PL model is represented with Equation 1 with two free parameters, where A denotes amplitude and α is the spectral index.

$$N_{\text{PL}}(E) = AE^{\alpha}. \quad (1)$$

The BAND function has four free parameters: low and high energy spectral indices, denoted as α and β respectively, the peak energy of νF_{ν} spectrum, denoted as E_{peak} , and amplitude, as shown in Equation 2.

$$N_{\text{BAND}}(E) = A \begin{cases} \left(\frac{E}{100 \text{ keV}}\right)^{\alpha} \exp\left[-\frac{(\alpha+2)E}{E_{\text{peak}}}\right], & E \geq \frac{(\alpha-\beta)E_{\text{peak}}}{\alpha+2} \\ \left(\frac{E}{100 \text{ keV}}\right)^{\beta} \exp(\beta-\alpha) \left[\frac{(\alpha-\beta)E_{\text{peak}}}{100 \text{ keV} (\alpha+2)}\right]^{\alpha-\beta}, & E < \frac{(\alpha-\beta)E_{\text{peak}}}{\alpha+2}. \end{cases} \quad (2)$$

CPL model is a subset of BAND model if β is very small and the part of $E < \frac{(\alpha-\beta)E_{\text{peak}}}{\alpha+2}$ of BAND model is ignored. There are three parameters in CPL model: the amplitude A , the lower energy index α , and the νF_{ν}

peak energy, E_{peak} , as shown in Equation 3.

$$N_{\text{COMP}}(E) = A \left(\frac{E}{E_{\text{piv}}} \right)^{\alpha} \exp \left[-\frac{(\alpha + 2)}{E_{\text{peak}}} E \right]. \quad (3)$$

The Equation 4 for the photon spectrum of a black body usually used in the spectral fitting, where $K = L_{39}/D_{\text{L},10\text{kpc}}^2$ is defined by the blackbody luminosity L in units of 10^{39} erg s $^{-1}$ in the GRB host galaxy frame and the luminosity distance D_{L} in units of 10 kpc.

$$N_{\text{BB}}(E) = \frac{K \times 8.0525 E^2}{(kT)^4 [\exp(E/kT) - 1]}. \quad (4)$$

All models are formulated in units of photon flux with energy (E) in keV and multiplied by a normalization constant A (ph s $^{-1}$ cm $^{-2}$ keV $^{-1}$), and kT and E are measured in the observer's frame. We determine the best spectral parameters by optimizing the Castor C statistic value. Castor Cstat (henceforth Cstat, Cash 1979) is a likelihood technique modified for a particular data set to converge to a χ^2 with an increase of the signal. χ^2 is evaluated for each spectral fit that is performed through minimizing C-Stat. **Among these 6 models, the best model is determined when a single additional parameter changes in χ^2 by at least 6 since the probability for achieving this difference is 0.01 as suggested by Goldstein et al. (2012), which is a conservative threshold to avoid the false positive rates of the extra component.**

As shown in Figure 18 in Appendix A, for GRB 200125B (HEB200125863), joint spectra fit with BAND model is the best model, with a reduced χ^2 of 1.14. A BAND model of low energy spectral index $\alpha = -0.78 \pm 0.01$, high energy spectral index $\beta = -2.70 \pm 0.03$, and the νF_{ν} peak energy, $E_{\text{peak}} = 200.8 \pm 7.7$ keV, is determined. GRB 210121A is observed by HXMT/CsI, *Fermi*/GBM and GECAM, and joint analysis with the other two missions is shown in Figure 21. $\alpha = -0.64 \pm 0.01$, $\beta = -2.49 \pm 0.03$ and $E_{\text{peak}} = 932.4 \pm 23.8$ keV are determined with a BAND model. Figure 22 shows the spectrum of GRB 210112A detected by *Swift*/BAT and HXMT/CsI. The best model is determined to be CPL, with $\alpha = -1.27 \pm 0.03$, and $E_{\text{peak}} = 347.7 \pm 49.7$ keV for the CPL component. In the case of utilizing data of *Swift*/BAT only, PL model is determined and the E_{peak} is not measured due to lack of information from higher energy band.

The distribution of energy spectra parameter of 'GOLDEN' GRBs are shown in Figures 7, 8, 9. Up to 29% low energy spectral indices of the 'GOLDEN' samples violate -2/3 synchrotron "line-of-death" (Preece

et al. 1998), while an additional 6% of the indices violate the -3/2 synchrotron cooling limit. The distribution of high-energy indices in Figure 9 peaks at a slope slightly steeper than -2 and have a extension toward steeper values. The E_{peak} distribution generally peaks around 200 keV, and spans over two orders of magnitude.

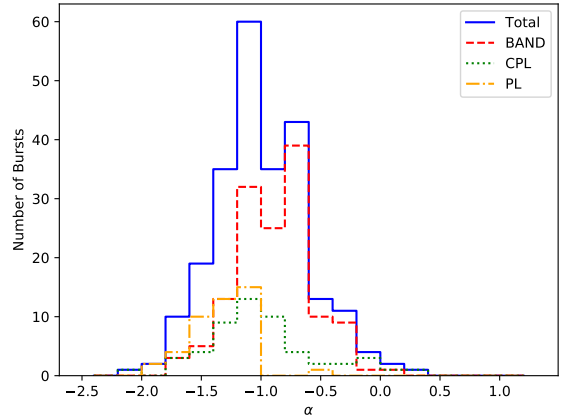


Figure 7. The distribution of low energy spectral index α of 'GOLDEN' GRBs from time-averaged spectral fits are shown. The blue solid lines denote the total distribution of α from BAND model (red dashed lines), CPL model (green dotted lines) and PL (orange dot-dashed lines).

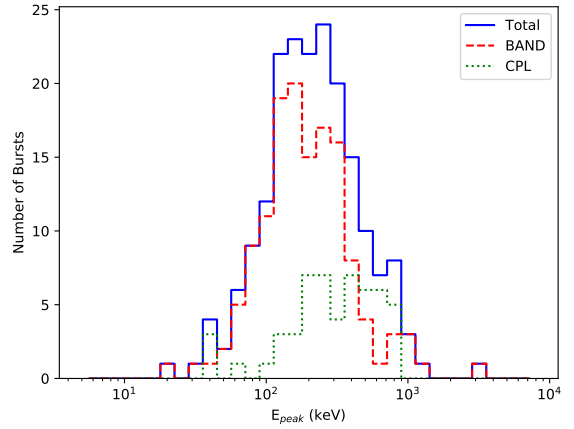


Figure 8. The distribution of νF_{ν} peak energy E_{peak} of 'GOLDEN' GRBs from time-averaged spectral fits are shown. The blue solid lines denote the total distribution of E_{peak} from BAND model (red dashed lines), CPL model (green dotted lines).

4.7.2. Duration and Fluence

For 'SILVER' and 'BRONZE' samples, the burst durations are determined by integrating the signal counts

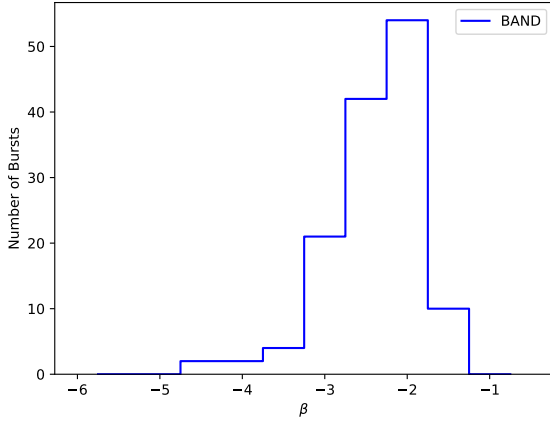


Figure 9. The distribution of high energy spectral index β of ‘GOLDEN’ GRBs from time-averaged spectral fits are shown.

from GRBs with deposited energy in ranges of 40-800 keV in NG mode and 200-3000 keV in LG mode, respectively. The duration T_{50} and T_{90} are determined from the interval between the times where the burst has reached 25% (5%) and 75% (95%) of its maximum counts. The method developed for BATSE (Koshut et al. 1996) are used to determine the systematic error. Table 5 shows the values of durations of ‘SILVER’ and ‘BRONZE’ samples.

For ‘GOLDEN’ samples, the burst durations T_{50} and T_{90} are computed in the 10-2000 keV energy range. They are determined using a method similar to that developed for BATSE (Koshut et al. 1996), the counts spectra of HXMT/CsI and the other missions in each time bin 64 ms are deconvolved and the durations are computed from the time history of fitted photon spectra, as shown in Figure 19 and 20. Peak fluxes of different time scales are naturally obtained in the same analysis, and the fluence is obtained by integrating the deconvolved flux history.

It is worth noting that, to avoid the failure of fit to each time bin, the parameters of GRB shape are fixed to the best model determined in joint fit to the time-averaged spectrum, while the amplitudes are set to be float. Therefore, in addition to the systematic effects mentioned in Koshut et al. (1996), an extra systematic error is introduced by fixed parameters. To estimate the uncertainty from the fixed parameters, we simulate tens of sets of parameters of the best GRB model by smearing the mean values with covariance matrix within one standard deviation. Then the same procedures are applied to calculate tens of sets of duration values. The maximum changes from the duration values with the

mean value are taken to be the systematic error from fixed GRB parameters. The systematic uncertainties of peak fluxes and fluences from the same source are also estimated in the same way. Note that in most cases of spectral parameters that are well determined, the system uncertainties of this kind are less than or numerically comparable with the the systematic effects, which could be ignored. As a sample of GRB 200125B, the total fluence (10-2000 keV) is $5.92\text{e-}05 \pm 4.54\text{e-}07 \text{ erg cm}^{-2}$, the peak flux ($\text{ph cm}^{-2} \text{ s}^{-1}$) in 10-2000 keV of timescales of 64 ms, 256 ms, 1024 ms is 175.35 ± 9.57 , 149.25 ± 3.78 , 110.27 ± 1.63 respectively.

5. CATALOG RESULTS

Table 3 lists the 322 searched bursts that are classified as GRBs. In the last column of Table 3, abbreviation of GRBs types are given. Among 322 searched bursts files, 202 ‘GOLDEN’ samples are analyzed and collected in all. 44 ‘SILVER’ , 50 ‘BRONZE’ and 26 ‘IRON’ samples are also listed in Table 2.

The results of the duration of GRBs are derived from joint analyses of HXMT with *Fermi*/GBM, *Swift*/BAT or GECAM discussed in 4.7, and shown in Table 4. The values of T_{50} and T_{90} in 10-2000 keV energy range are listed along with their respective statistical error estimates and start times relative to the trigger time of HXMT. As part of the duration analysis, peak fluxes and fluence are computed. Table 6 shows the total fluence and peak fluxes of different time scales in 10-2000 keV. Table 5 lists the durations of ‘SILVER’ and ‘GOLDEN’ samples, which obtained from HXMT/CsI GRBs signal counts.

6. DISCUSSION AND SUMMARY

Histograms of the T_{50} and T_{90} distributions are shown in 10-2000 keV energy range in Figure 10. Using the conventional division between the short and long GRB classes ($T_{90}=2$ s), we find 35 (17%) of the 202 ‘GOLDEN’ GRBs to be in the short regime. Within the quoted duration errors, the number of short GRB events ranges from 28 (14%) to 39 (19%). It is consistent with the results from *Fermi*/GBM GRB catalogs covering ten years (von Kienlin et al. 2020), which has 395 (17%) short GRBs from statistics in 10-1000 keV. Due to the limited statistic of GRB numbers, we do not perform lognormal fits to the distribution of durations.

Figure 16 shows the comparison of durations (T_{90}) from joint analyses with other missions and those from HXMT/CsI GRBs data, where the red line denotes the case of these two are equivalent to each other. **Most GRBs are below the red line, because energy range of HXMT/CsI is higher than those of other**

missions, such as *Fermi*/GBM and that GRBs tend to be shorter at higher energy. Therefore, joint analysis is necessary for the measurement of duration in 10-2000 keV.

Despite of the limited statistic of ‘GOLDEN’ GRBs, as shown in Figure 11, anti-correlation of spectral hardness with duration is confirmed by the relationship between the hardness and duration, where the hardness is calculated as the ratio of the flux density from spectral parameters determined from time-averaged spectral fits in 50-300 keV to that in 10-50 keV. We note that, here the durations are those from joint analyses in energy range of 10-2000 keV, which also illustrates the anti-correlation between the hardness of GRBs spectra and duration.

Distributions of GRBs fluence are shown in Figure 15. Peak fluxes on timescales of 64 ms, 256 ms, 1024 ms are shown in Figure 12, Figure 13 and Figure 14 respectively. These distributions are not consistent with those from von Kienlin et al. (2020). The contributions are very small both below 10^{-7} erg cm $^{-2}$ and 1 ph cm $^{-2}$ s $^{-1}$ in distributions of fluence and peak fluxes. It could be explained by the sharply fall of effective area below 100 keV. Weak short GRBs cannot cause enough statistics in HXMT/CsI, and thus cannot be detected significantly. Extremely bright GRBs would not be included in ‘GOLDEN’ samples because they are very likely to cause data saturation in HXMT and be labeled as ‘IRON’ samples.

This work made use of the data from the *Insight-HXMT* mission, a project funded by China National Space Administration (CNSA) and the Chinese Academy of Sciences (CAS). The authors thank supports from the National Program on Key Research and Development Project (Grants No. 2016YFA0400801, 2021YFA0718500), the National Natural Science Foundation of China under Grants No. U1838113, and the Strategic Priority Research Program on Space Science, the Chinese Academy of Sciences (Grant No. XDB23040400, XDA15052700). The authors are very grateful to the public data of *Fermi*/GBM, *Swift*/BAT and GECAM.

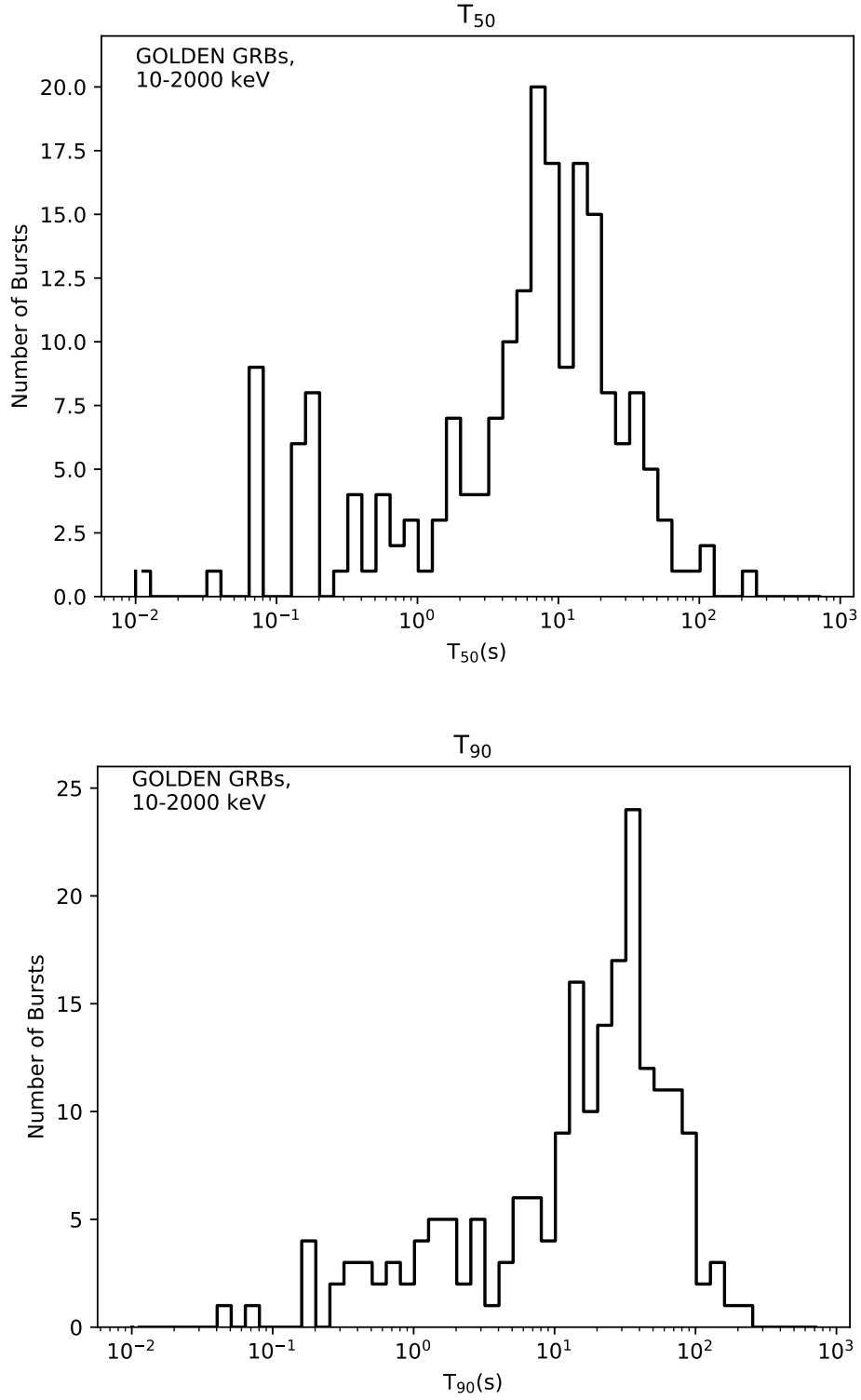


Figure 10. Distributions of ‘GOLDEN’ GRB durations in the 10-2000 keV energy range are shown. The upper plot shows T_{50} and the lower plot shows T_{90} .

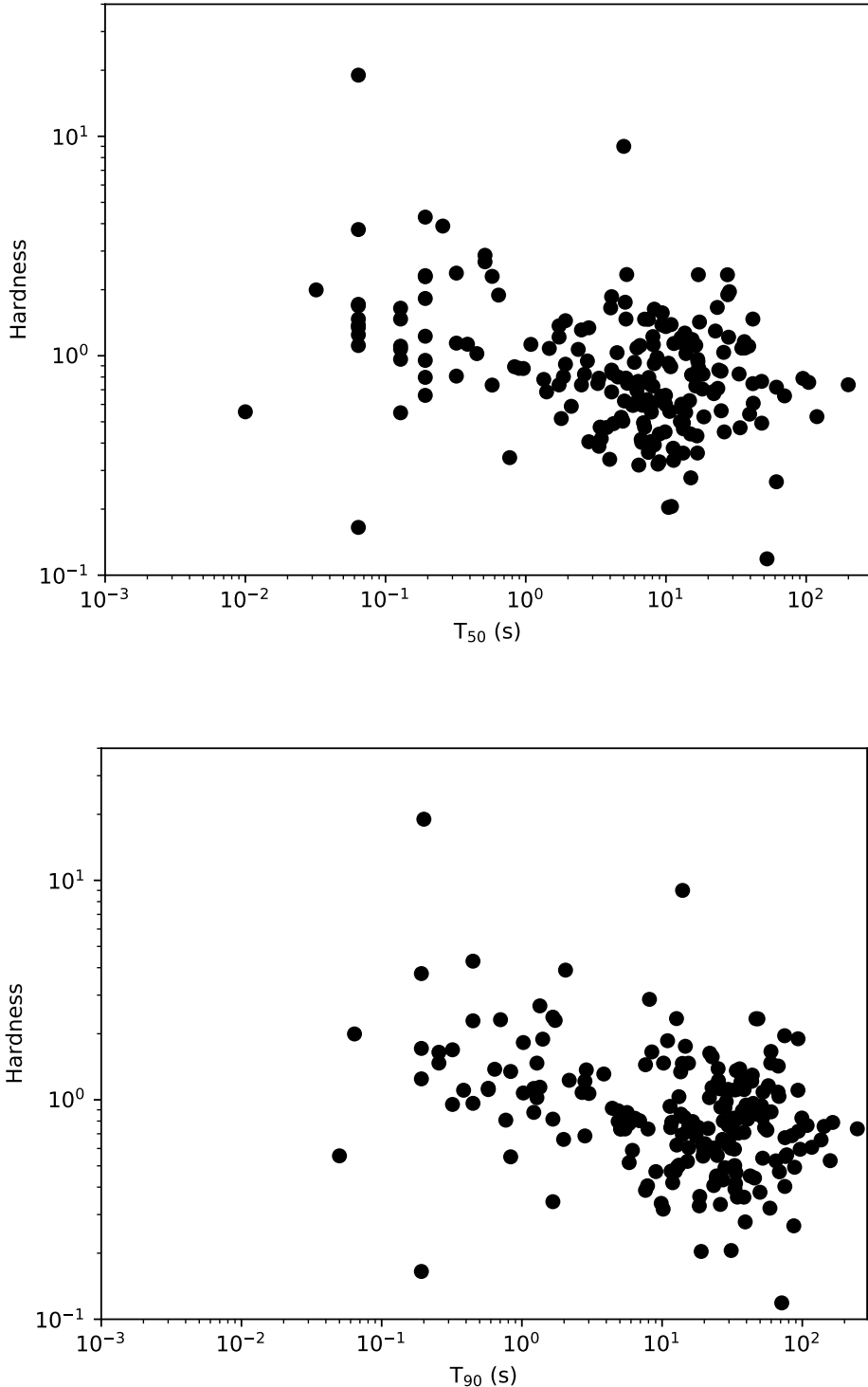


Figure 11. Scatter plots of spectral hardness vs. duration are shown for the two duration measures T_{50} (upper plot) and T_{90} (lower plot) as shown in Figure 10. The hardness is calculated as the ratio of the flux density from spectral parameters determined from time-averaged spectral fits in 50-300 keV to that in 10-50 keV. For clarity, the estimated errors are not shown but can be quite large for the weak events. Nevertheless, the anti-correlation of spectral hardness with burst duration is evident.

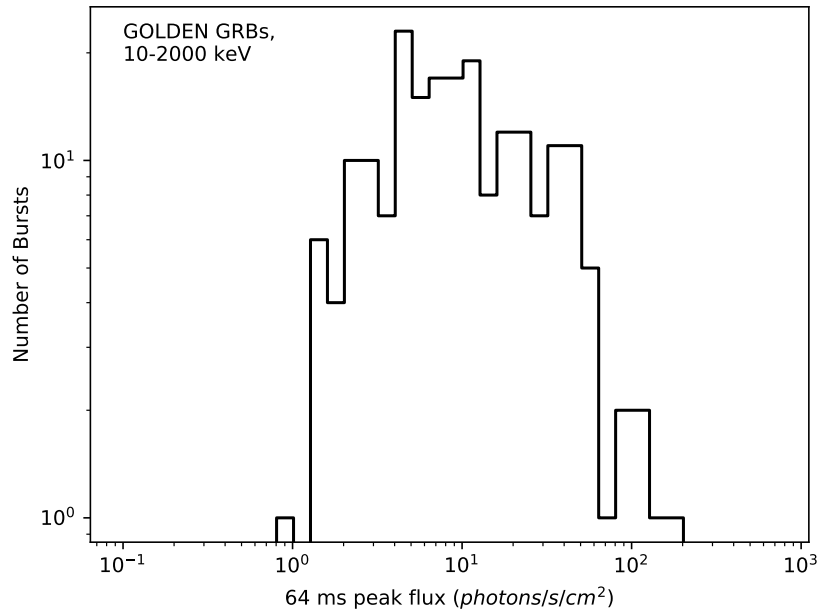


Figure 12. Distribution of ‘GOLDEN’ GRBs peak flux on the 0.064 s timescale is shown in energy range of 10-2000 keV.

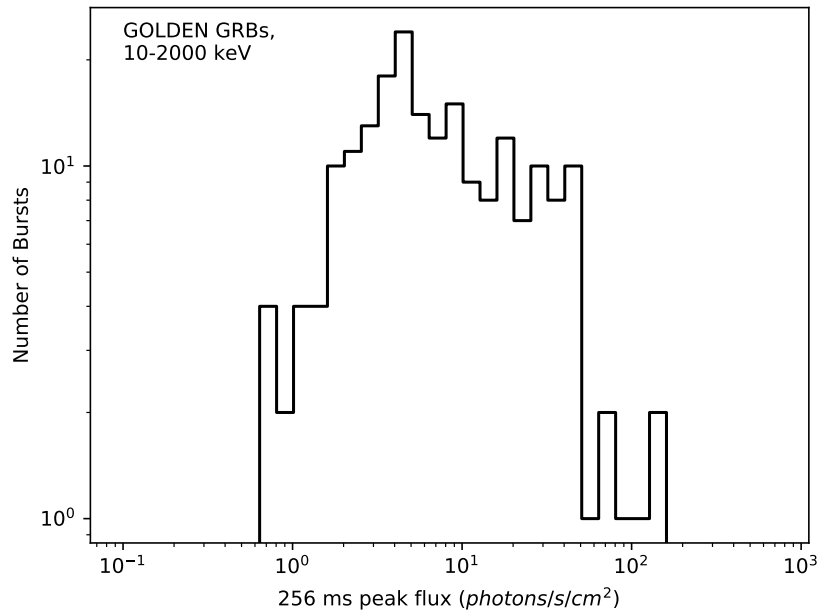


Figure 13. Distribution of ‘GOLDEN’ GRBs peak flux on the 0.256 s timescale is shown in energy range of 10-2000 keV.

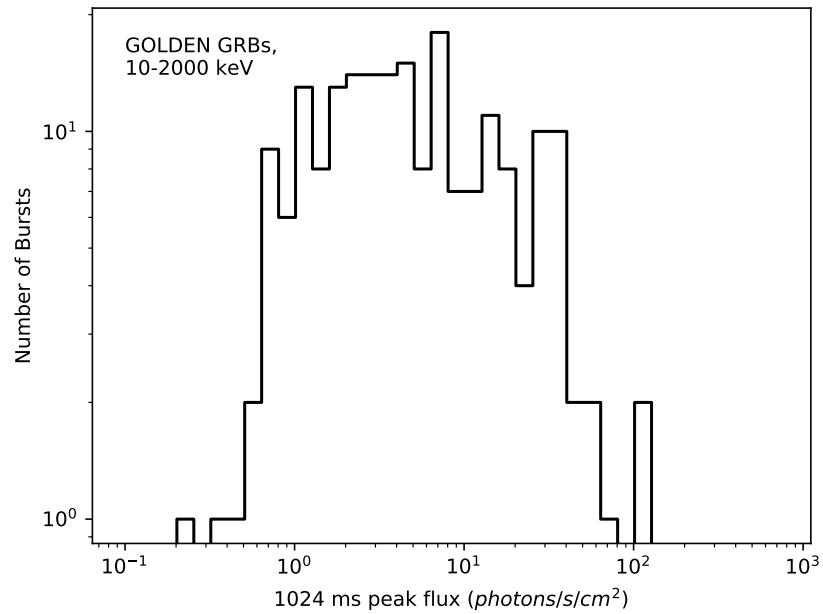


Figure 14. Distribution of ‘GOLDEN’ GRBs peak flux on 1.024 s timescale is shown in energy range of 10-2000 keV.

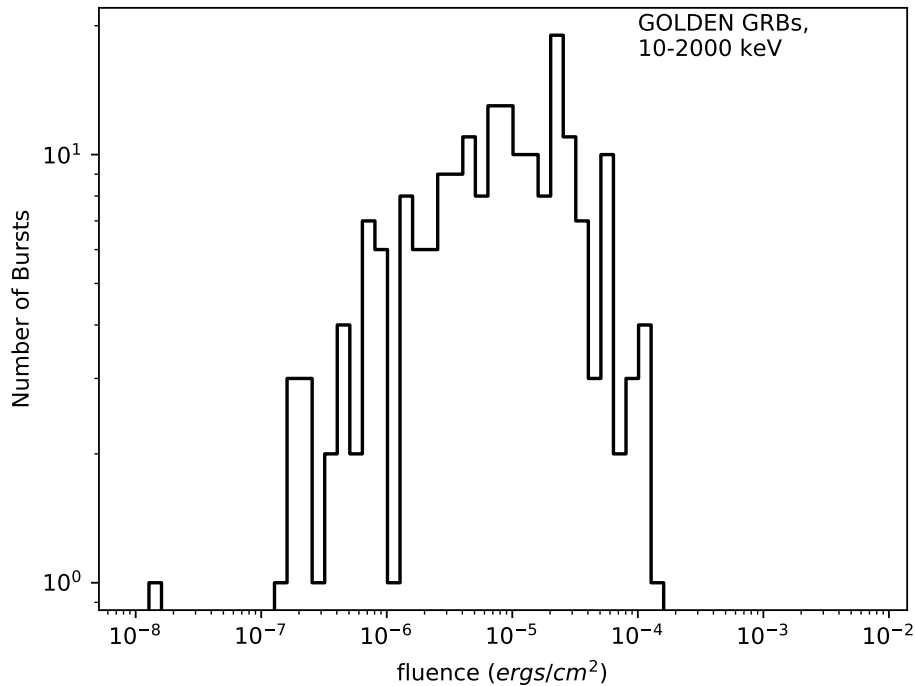


Figure 15. Distribution of ‘GOLDEN’ GRBs fluence is shown in energy range of 10-2000 keV.

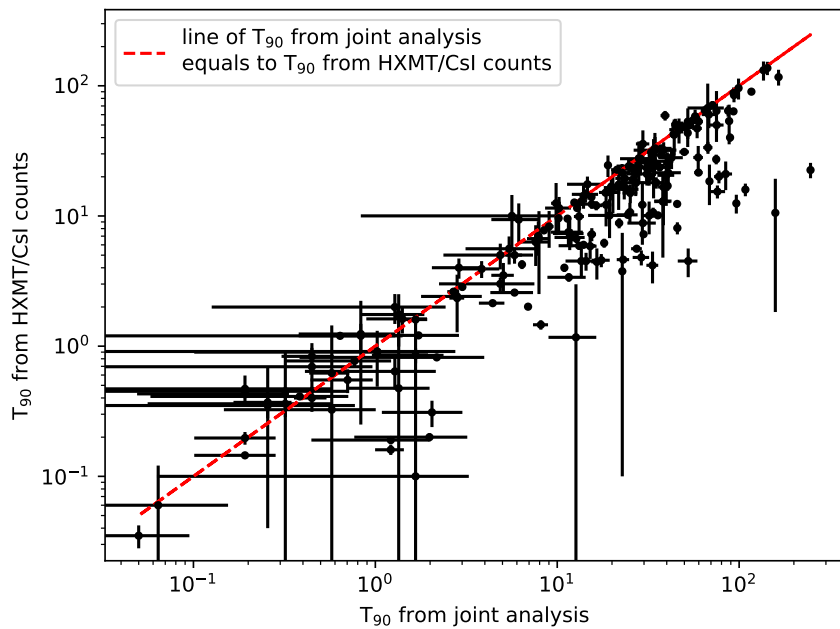


Figure 16. A comparison between the durations (T_{90}) of ‘GOLDEN’ GRBs from joint analysis and those obtained from HXMT/CsI GRBs counts are shown. The red line denotes the case of these two are equal to each other.

Table 3. GRB Triggers: Locations and Trigger Characteristics.

Trigger ID ^a	GRB Name	Trigger Time (UTC)	Search Method ^b	Gain Mode	RA(°)	DEC(°)	err(°)	location source ^c	Kinds of GRB samples ^d
HEB170626040	GRB 170626B	2017-06-26T00:57:55.80	BLIND	NG	289.8	-19.2	5.0	IPN	S
HEB170626400	GRB 170626A	2017-06-26T09:37:22.32	BLIND	NG	165.4	56.5	1.0	Fermi/GBM	G
HEB170705115	GRB 170705A	2017-07-05T02:45:59.00	BLIND	NG	191.7	18.3	0.1	Swift	G
HEB170708045	GRB 170708A	2017-07-08T01:06:11.25	BLIND	LG	335.8	19.8	4.6	IPN	S
HEB170712139	GRB 170712A	2017-07-12T03:20:30.00	BLIND	LG	-	-	-	-	B
HEB170714049	GRB 170714B	2017-07-14T01:10:51.10	BLIND	NG	18.2	29.5	-	Fermi/GBM	G
HEB170718152	-	2017-07-18T03:39:30.00	TARGETED	NG	102.3	-35.0	-	Fermi/GBM	G
HEB170726248	GRB 170726B	2017-07-26T05:58:15.42	BLIND	NG	166.4	-34.0	2.8	Fermi/GBM	G
HEB170726793	GRB 170726A	2017-07-26T19:02:59.51	BLIND	NG	297.8	6.6	-	Fermi/GBM	G
HEB170728960	GRB 170728B	2017-07-28T23:03:19.00	BLIND	NG	238.0	70.1	-	Fermi/GBM	G
HEB170731751	-	2017-07-31T18:01:39.75	BLIND	NG	245.2	64.3	6.3	Fermi/GBM	G
HEB170801208	GRB 170801A	2017-08-01T04:59:55.25	BLIND	NG	-	-	-	-	B
HEB170802637	GRB 170802A	2017-08-02T15:18:26.00	BLIND	NG	52.3	-39.2	2.1	Fermi/GBM	G
HEB170803917	GRB 170803B	2017-08-03T22:00:31.00	BLIND	NG	-	-	-	-	S
HEB170805596	GRB 170805B	2017-08-05T14:18:49.50	BLIND	NG	137.3	69.6	1.3	IPN	S
HEB170805610	GRB 170805A	2017-08-05T14:38:34.00	BLIND	NG	269.2	-18.3	4.6	IPN	S
HEB170817908	GRB 170817B	2017-08-17T21:47:34.00	BLIND	NG	83.0	50.1	3.7	Fermi/GBM	G
HEB170825306	-	2017-08-25T07:22:03.00	BLIND	NG	274.4	-26.2	3.2	Fermi/GBM	G
HEB170826818	GRB 170826B	2017-08-26T19:38:58.00	BLIND	NG	327.7	-31.8	1.0	Fermi/GBM	G
HEB170829270	GRB 170829A	2017-08-29T06:29:39.90	BLIND	NG	-	-	-	-	S
HEB170901499	GRB 170901B	2017-09-01T11:59:56.50	BLIND	NG	-	-	-	-	B
HEB170903534	GRB 170903A	2017-09-03T12:49:11.00	BLIND	LG	254.5	35.0	1.3	Fermi/GBM	G
HEB170904406	GRB 170904A	2017-09-04T09:46:00.62	BLIND	NG	35.4	-32.5	3.2	IPN	S
HEB170904884	-	2017-09-04T21:13:07.10	BLIND	NG	-	-	-	-	B
HEB170906029	GRB 170906A	2017-09-06T00:43:06.00	BLIND	LG	198.6	-53.5	12.2	Fermi/GBM	G
HEB170912984	GRB 170912C	2017-09-12T23:38:12.60	BLIND	NG	83.6	7.2	-	Fermi/GBM	G
HEB170918905	GRB 170918A	2017-09-18T21:43:35.40	BLIND	NG	-	-	-	-	B
HEB170921030	GRB 170921C	2017-09-21T00:43:37.00	BLIND	NG	-	-	-	-	B
HEB170923188	GRB 170923A	2017-09-23T04:31:05.44	BLIND	NG	221.5	81.2	5.0	Fermi/GBM	G
HEB170926340	GRB 170926A	2017-09-26T08:10:39.80	BLIND	NG	-	-	-	-	B
HEB171007498	GRB 171007A	2017-10-07T11:57:38.27	BLIND	NG	135.6	42.8	0.1	Swift	I
HEB171008079	GRB 171008A	2017-10-08T01:54:38.50	BLIND	NG	232.6	24.0	-	Fermi/GBM	G
HEB17101045	GRB 171011B	2017-10-11T01:05:36.00	BLIND	NG	158.9	1.6	8.1	IPN	I

Table 3 continued

Table 3 (*continued*)

Trigger ID ^a	GRB Name	Trigger Time (UTC)	Search Method ^b	Gain Mode	RA(°)	DEC(°)	err(°)	location source ^c	Kinds of GRB samples ^d
HEB171013350	GRB 171013B	2017-10-13T08:24:42.11	TARGETED	NG	145.1	-32.6	30.3	Fermi/GBM	G
HEB171020963	GRB 171020A	2017-10-20T23:07:10.75	BLIND	NG	39.2	15.2	0.1	Swift	G
HEB171030728	GRB 171030A	2017-10-30T17:29:45.00	BLIND	NG	74.1	-19.5	23.4	IPN	G
HEB17102106	GRB 17102A	2017-11-02T02:33:35.99	BLIND	NG	188.8	54.3	11.5	IPN	S
HEB171103965	GRB 171103A	2017-11-03T23:10:30.04	BLIND	NG	249.5	-10.2	3.0	Fermi/GBM	G
HEB171108279	GRB 171108B	2017-11-08T06:42:24.00	BLIND	NG	-	-	-	-	B
HEB171115217	GRB 171115B	2017-11-15T05:13:14.70	BLIND	NG	-	-	-	-	B
HEB171120555	GRB 171120A	2017-11-20T13:20:02.00	BLIND	NG	163.8	22.5	0.1	Swift	G
HEB171124234	GRB 171124A	2017-11-24T05:38:03.00	BLIND	NG	333.9	35.1	1.6	Fermi/GBM	G
HEB171207054	-	2017-12-07T01:18:42.45	TARGETED	NG	314.4	51.7	9.5	Fermi/GBM	G
HEB171209615	GRB 171209A	2017-12-09T14:46:16.22	BLIND	NG	139.4	-30.5	0.1	Swift	G
HEB171210492	GRB 171210A	2017-12-10T11:49:16.00	BLIND	NG	338.0	27.5	1.0	Fermi/GBM	G
HEB171215705	GRB 171215A	2017-12-15T16:55:26.57	BLIND	NG	19.7	34.7	4.7	Fermi/GBM	G
HEB171223818	GRB 171223A	2017-12-23T19:38:15.00	BLIND	NG	115.8	-33.5	6.6	Fermi/GBM	G
HEB171230955	GRB 171230B	2017-12-30T22:55:34.00	BLIND	NG	89.5	-27.8	1.1	Fermi/GBM	G
HEB180103047	GRB 180103A	2018-01-03T01:08:40.00	BLIND	NG	159.6	-53.5	0.1	Swift	S
HEB180103949	-	2018-01-03T23:47:12.00	BLIND	NG	-	-	-	-	B
HEB180110608	-	2018-01-10T14:35:59.22	BLIND	NG	126.3	51.3	30.1	Fermi/GBM	G
HEB180111695	GRB 180111A	2018-01-11T16:42:06.38	BLIND	LG	149.8	48.2	0.1	Swift	G
HEB180112687	GRB 180112A	2018-01-12T16:30:38.00	BLIND	LG	-	-	-	-	S
HEB180113011	GRB 180113B	2018-01-13T00:16:00.00	BLIND	NG	354.0	13.5	1.2	Fermi/GBM	I
HEB180113418	GRB 180113C	2018-01-13T10:02:07.50	BLIND	NG	174.6	-64.7	1.0	Fermi/GBM	I
HEB180119836	-	2018-01-19T20:04:49.78	BLIND	NG	348.7	-15.0	2.5	Fermi/GBM	G
HEB180127049	-	2018-01-27T01:11:12.91	BLIND	NG	20.5	25.8	5.0	Fermi/GBM	G
HEB180130744	-	2018-01-30T17:51:26.79	TARGETED	NG	136.8	52.7	68.1	Fermi/GBM	G
HEB180202211	GRB 180202A	2018-02-02T05:04:28.00	BLIND	NG	-	-	-	-	S
HEB180208764	-	2018-02-08T18:20:50.30	TARGETED	NG	196.6	8.2	5.1	Fermi/GBM	G
HEB180210517	GRB 180210A	2018-02-10T12:24:44.00	BLIND	NG	3.3	21.0	1.5	Fermi/GBM	G
HEB180210728	-	2018-02-10T17:29:06.00	BLIND	NG	-	-	-	-	B
HEB180218634	GRB 180218A	2018-02-18T15:14:05.49	BLIND	NG	47.2	46.6	4.4	Fermi/GBM	I
HEB180219482	GRB 180219A	2018-02-19T11:34:39.00	BLIND	NG	86.2	32.3	1.0	Fermi/GBM	I
HEB180221520	GRB 180221B	2018-02-21T12:30:01.00	BLIND	NG	-	-	-	-	S
HEB180226392	-	2018-02-26T09:24:58.73	BLIND	NG	45.9	31.2	1.6	Fermi/GBM	G
HEB180305393	GRB 180305A	2018-03-05T09:26:08.66	TARGETED	NG	196.8	-32.2	14.8	Fermi/GBM	G
HEB180306972	-	2018-03-06T23:20:33.93	TARGETED	NG	-	-	-	-	-

Table 3 *continued*

Table 3 (*continued*)

Trigger ID ^a	GRB Name	Trigger Time (UTC)	Search Method ^b	Gain Mode	RA(°)	DEC(°)	err(°)	location source ^c	Kinds of GRB samples ^d
HEB180309321	-	2018-03-09T07:43:10.62	TARGETED	NG	186.1	34.5	2.1	Fermi/GBM	G
HEB180313977	GRB 180313A	2018-03-13T23:28:17.53	BLIND	NG	317.5	-26.5	5.7	Fermi/GBM	G
HEB180326143	GRB 180326A	2018-03-26T03:26:07.06	BLIND	NG	291.7	-13.5	3.1	IPN	S
HEB180330891	-	2018-03-30T21:23:15.52	BLIND	NG	164.2	83.9	3.7	Fermi/GBM	G
HEB180331177	GRB 180331A	2018-03-31T04:14:55.70	BLIND	NG	66.0	13.4	0.1	Swift	G
HEB180401279	-	2018-04-01T06:42:43.78	BLIND	NG	126.7	7.0	1.6	Fermi/GBM	G
HEB180402406	GRB 180402A	2018-04-02T09:44:59.37	BLIND	NG	251.9	-14.9	0.1	Swift	G
HEB180404091	GRB 180404B	2018-04-04T02:11:38.64	BLIND	NG	53.0	-49.3	1.2	Fermi/GBM	G
HEB180405168	-	2018-04-05T04:02:53.06	BLIND	NG	123.6	-33.5	2.2	Fermi/GBM	S
HEB180409346	GRB 180409A	2018-04-09T08:18:18.67	BLIND	LG	178.2	36.0	1.0	Fermi/GBM	G
HEB180411359	GRB 180411B	2018-04-11T08:37:29.76	BLIND	NG	-	-	-	-	B
HEB180413117	-	2018-04-13T02:49:43.23	BLIND	NG	168.2	-31.6	1.2	Fermi/GBM	G
HEB180416923	GRB 180416B	2018-04-16T22:10:11.00	BLIND	NG	353.5	74.6	2.1	Fermi/GBM	G
HEB180427442	GRB 180427A	2018-04-27T10:37:03.00	BLIND	NG	283.3	46.6	1.0	Fermi/GBM	G
HEB180505539	GRB 180505A	2018-05-05T12:57:30.00	BLIND	LG	4.5	-59.9	1.2	Fermi/GBM	G
HEB180506902	-	2018-05-06T21:38:58.00	BLIND	NG	61.2	-0.9	6.7	Fermi/GBM	G
HEB180510898	GRB 180510A	2018-05-10T19:24:39.00	BLIND	NG	276.3	-31.9	1.0	Swift	G
HEB180523782	-	2018-05-23T18:46:28.00	BLIND	LG	168.4	49.4	12.9	Fermi/GBM	G
HEB180525151	-	2018-05-25T03:37:59.05	BLIND	NG	103.3	19.9	14.9	Fermi/GBM	G
HEB180603235	-	2018-06-03T05:39:50.00	BLIND	LG	-	-	-	-	S
HEB180605457	GRB 180605A	2018-06-05T10:59:25.00	BLIND	LG	50.0	-50.4	1.0	Fermi/GBM	G
HEB180615462	-	2018-06-15T11:05:56.00	BLIND	NG	55.8	78.3	1.0	Fermi/GBM	I
HEB180617871	-	2018-06-17T20:55:23.60	BLIND	NG	-	-	-	-	B
HEB180618030	GRB 180618A	2018-06-18T00:43:13.00	BLIND	NG	169.9	73.8	0.1	Swift	G
HEB180623696	GRB 180623A	2018-06-23T16:42:21.00	BLIND	NG	214.5	-60.3	0.1	Swift	G
HEB180625940	-	2018-06-25T22:34:41.50	BLIND	NG	39.1	-62.3	6.4	Fermi/GBM	G
HEB180626260	GRB 180626D	2018-06-26T06:15:14.00	BLIND	NG	-	-	-	-	B
HEB180626391	GRB 180626C	2018-06-26T09:23:50.95	BLIND	NG	285.1	44.8	8.2	Fermi/GBM	G
HEB180704233	GRB 180704A	2018-07-04T05:36:43.00	BLIND	NG	32.6	70.0	0.1	Swift	G
HEB180704525	GRB 180704B	2018-07-04T12:36:33.00	BLIND	NG	-	-	-	Fermi/GBM	S
HEB180715754	GRB 180715A	2018-07-15T18:07:05.00	BLIND	NG	231.8	-4.4	4.8	Fermi/GBM	G
HEB180718762	GRB 180718B	2018-07-18T18:18:24.00	BLIND	NG	44.7	-31.5	0.6	Fermi/LAT	G
HEB180720598	GRB 180720B	2018-07-20T14:21:39.65	BLIND	LG	0.5	-2.9	1.2	Fermi/GBM	I
HEB180722992	GRB 180722B	2018-07-22T23:49:13.00	BLIND	NG	55.3	41.7	3.5	Fermi/GBM	G
HEB180724807	GRB 180724A	2018-07-24T19:22:31.00	BLIND	LG	285.2	-33.7	1.0	Fermi/GBM	G

Table 3 continued

Table 3 (*continued*)

Trigger ID ^a	GRB Name	Trigger Time (UTC)	Search Method ^b	Gain Mode	RA(°)	DEC(°)	err(°)	location source ^c	Kinds of GRB samples ^d
HEB180730017	-	2018-07-30T00:25:40.00	BLIND	NG	98.0	44.5	8.3	Fermi/GBM	G
HEB180801275	-	2018-08-01T06:37:03.51	TARGETED	NG	240.9	-11.4	8.8	Fermi/GBM	G
HEB180803590	-	2018-08-03T14:09:49.73	BLIND	LG	71.6	57.6	17.4	Fermi/GBM	G
HEB180804554	-	2018-08-04T13:17:48.00	BLIND	NG	-	-	-	-	B
HEB180804930	-	2018-08-04T22:20:38.28	BLIND	NG	109.4	-69.3	1.8	Fermi/GBM	G
HEB180816088	-	2018-08-16T02:07:18.91	TARGETED	NG	126.2	-36.7	1.9	Fermi/GBM	G
HEB180822561	-	2018-08-22T13:28:34.05	TARGETED	NG	185.2	-61.5	2.2	Fermi/GBM	G
HEB180828759	GRB 180828A	2018-08-28T18:57:26.58	BLIND	NG	270.7	-23.9	1.2	Fermi/GBM	G
HEB180912273	-	2018-09-12T06:34:15.40	BLIND	NG	202.0	-26.2	2.1	Fermi/GBM	I
HEB180914765	GRB 180914B	2018-09-14T18:22:48.00	BLIND	NG	332.4	24.9	0.3	Fermi/LAT	I
HEB180922461	-	2018-09-22T11:03:52.02	TARGETED	NG	19.2	-0.1	4.4	Fermi/GBM	I
HEB180925407	-	2018-09-25T09:46:30.54	TARGETED	NG	181.9	-25.4	9.3	Fermi/GBM	G
HEB180925609	GRB 180925A	2018-09-25T14:37:27.90	BLIND	NG	315.2	-64.4	0.1	Swift	G
HEB180927792	-	2018-09-27T23:49:20.19	BLIND	NG	236.0	-1.7	5.7	Fermi/GBM	G
HEB180929453	-	2018-09-29T10:52:33.92	BLIND	NG	244.7	-8.9	8.4	Fermi/GBM	G
HEB181008269	-	2018-10-08T06:28:13.50	BLIND	NG	57.5	7.2	14.4	Fermi/GBM	G
HEB181011181	-	2018-10-11T04:21:12.00	BLIND	LG	-	-	-	-	S
HEB181014479	-	2018-10-14T11:30:23.00	BLIND	LG	228.9	16.5	1.3	Fermi/GBM	G
HEB181028590	GRB 181028A	2018-10-28T14:09:43.00	BLIND	LG	88.9	-21.2	2.5	IPN	G
HEB181112582	-	2018-11-12T13:58:51.00	BLIND	NG	-	-	-	-	I
HEB181119605	GRB 181119A	2018-11-19T14:32:17.13	BLIND	NG	86.4	37.1	1.8	Fermi/GBM	G
HEB181121306	-	2018-11-21T07:21:29.27	BLIND	NG	130.9	31.5	18.3	Fermi/GBM	G
HEB181122381	-	2018-11-22T09:09:03.06	BLIND	LG	93.7	34.4	4.2	Fermi/GBM	G
HEB181123231	GRB 181123B	2018-11-23T05:33:03.09	BLIND	NG	184.3	14.6	0.1	Swift	G
HEB181201111	GRB 181201A	2018-12-01T02:39:53.00	BLIND	NG	319.3	-12.6	0.1	IBIS	S
HEB181212692	GRB 181212A	2018-12-12T16:37:45.50	BLIND	NG	298.4	-3.7	2.3	Fermi/GBM	G
HEB181213540	GRB 181213A	2018-12-13T12:57:38.00	BLIND	NG	248.3	78.5	0.1	Swift	G
HEB181217664	GRB 181217A	2018-12-17T15:56:57.00	BLIND	NG	332.2	29.9	-	Fermi/GBM	G
HEB181222841	GRB 181222B	2018-12-22T20:11:37.00	BLIND	NG	311.1	22.9	1.6	Fermi/GBM	I
HEB181225489	GRB 181225A	2018-12-25T11:44:10.00	BLIND	LG	348.1	-9.5	-	Fermi/GBM	G
HEB190102652	-	2019-01-02T15:40:17.27	BLIND	NG	-	-	-	-	S
HEB190103695	GRB 190103A	2019-01-03T16:41:52.64	BLIND	NG	251.4	17.4	2.7	IPN	I
HEB190103877	GRB 190103B	2019-01-03T21:03:50.00	BLIND	NG	212.6	35.3	0.1	Swift	G
HEB190110725	GRB 190110A	2019-01-10T17:24:53.00	BLIND	NG	277.0	-49.2	2.2	Fermi/GBM	G
HEB190114872	GRB 190114C	2019-01-14T20:57:02.00	BLIND	LG	56.2	-31.8	3.3	Fermi/GBM	I

Table 3 *continued*

Table 3 (*continued*)

Trigger ID ^a	GRB Name	Trigger Time (UTC)	Search Method ^b	Gain Mode	RA(°)	DEC(°)	err(°)	location source ^c	Kinds of GRB samples ^d
HEB190117608	GRB 190117A	2019-01-17T14:36:47.00	BLIND	NG	-	-	-	-	S
HEB190131964	GRB 190131A	2019-01-31T23:08:35.00	BLIND	NG	42.3	35.5	2.2	Fermi/GBM	G
HEB190203655	-	2019-02-03T15:44:09.00	BLIND	NG	-	-	-	-	B
HEB190212129	GRB 190212A	2019-02-12T03:06:20	BLIND	NG	-	-	-	-	S
HEB190215771	GRB 190215A	2019-02-15T18:31:22.48	BLIND	NG	342.3	36.2	1.0	Fermi/GBM	G
HEB190218810	-	2019-02-18T19:27:40.00	BLIND	NG	-	-	-	-	B
HEB190222537	-	2019-02-22T12:53:27.15	BLIND	NG	147.3	60.9	1.5	Fermi/GBM	G
HEB190226515	GRB 190226A	2019-02-26T12:21:45.50	BLIND	NG	224.4	-8.6	-	Fermi/GBM	G
HEB190305545	GRB 190305A	2019-03-05T13:05:19.00	BLIND	NG	-	-	-	-	I
HEB190306467	GRB 190306B	2019-03-06T11:13:27.95	BLIND	NG	-	-	-	-	B
HEB190310398	GRB 190310A	2019-03-10T09:33:25.00	BLIND	NG	349.3	12.1	1.2	Fermi/GBM	G
HEB190321931	GRB 190321A	2019-03-21T22:21:21.00	BLIND	NG	-	-	-	-	S
HEB190323878	GRB 190323D	2019-03-23T21:05:24.00	BLIND	NG	34.7	10.3	1.1	Fermi/GBM	S
HEB190324348	GRB 190324B	2019-03-24T08:21:21.00	BLIND	NG	81.0	12.0	1.0	Fermi/GBM	G
HEB190324947	GRB 190324A	2019-03-24T22:44:20.50	BLIND	NG	49.6	-47.2	0.1	Swift	G
HEB190326313	GRB 190326B	2019-03-26T07:31:47.00	BLIND	NG	264.2	68.3	1.3	Fermi/GBM	G
HEB190326316	GRB 190326A	2019-03-26T07:35:28.90	BLIND	NG	341.6	39.9	0.1	Swift	G
HEB190330207	-	2019-03-30T04:59:27.70	BLIND	NG	-	-	-	-	B
HEB190330694	GRB 190330A	2019-03-30T16:39:32.00	BLIND	LG	86.9	22.6	2.1	Fermi/GBM	G
HEB190331093	GRB 190331A	2019-03-31T02:14:38.00	BLIND	NG	28.6	27.6	0.1	Swift	G
HEB190331841	GRB 190331C	2019-03-31T20:12:00.10	BLIND	NG	-	-	-	-	S
HEB190401139	GRB 190401A	2019-04-01T03:20:21.00	BLIND	NG	280.0	39.0	5.7	Fermi/GBM	G
HEB190407671	GRB 190407A	2019-04-07T16:07:26.49	TARGETED	NG	181.8	40.6	4.5	Fermi/GBM	G
HEB190411406	GRB 190411A	2019-04-11T09:45:46.00	BLIND	NG	286.0	-36.3	4.8	Fermi/GBM	I
HEB190415173	GRB 190415A	2019-04-15T04:09:49.90	BLIND	NG	26.9	13.9	6.6	Fermi/GBM	I
HEB190422283	-	2019-04-22T06:48:17.50	BLIND	NG	306.7	-73.0	1.8	Fermi/GBM	S
HEB190424417	GRB 190424A	2019-04-24T10:00:42.00	BLIND	NG	48.7	20.2	0.1	Swift	G
HEB190507269	GRB 190507A	2019-05-07T06:28:23.00	BLIND	NG	156.0	-12.8	4.8	Fermi/GBM	G
HEB190510119	GRB 190510B	2019-05-10T02:52:13.23	TARGETED	NG	124.5	-53.1	1.2	Fermi/GBM	S
HEB190515189	GRB 190515A	2019-05-15T04:33:03.00	BLIND	NG	137.2	39.3	5.0	Fermi/GBM	G
HEB190525031	GRB 190525A	2019-05-25T00:45:47.65	TARGETED	NG	338.0	5.4	4.0	Fermi/GBM	G
HEB190530429	GRB 190530A	2019-05-30T10:19:08.90	BLIND	NG	120.5	35.5	1.0	Fermi/GBM	I
HEB190531840	GRB 190531B	2019-05-31T20:10:12.00	BLIND	NG	24.3	-42.0	1.0	Fermi/GBM	G
HEB190604446	GRB 190604A	2019-06-04T10:42:37.05	BLIND	NG	342.5	46.4	1.0	Fermi/GBM	G
HEB190605110	GRB 190605B	2019-06-05T02:39:08.00	BLIND	NG	-	-	-	-	B

Table 3 continued

Table 3 (*continued*)

Trigger ID ^a	GRB Name	Trigger Time (UTC)	Search Method ^b	Gain Mode	RA(°)	DEC(°)	err(°)	location source ^c	Kinds of GRB samples ^d
HEB190606079	GRB 190606A	2019-06-06T01:55:07.78	BLIND	NG	76.6	-0.6	6.0	IPN	I
HEB190610477	GRB 190610A	2019-06-10T11:27:45.00	BLIND	NG	46.2	-7.7	0.1	Swift	S
HEB190613449	GRB 190613B	2019-06-13T10:47:00.00	BLIND	NG	305.4	-4.6	0.1	Swift	G
HEB190615612	GRB 190615B	2019-06-15T14:42:22.00	BLIND	NG	-	-	-	-	B
HEB190615636	GRB 190615A	2019-06-15T15:16:27.00	BLIND	NG	191.4	49.4	2.3	Fermi/GBM	G
HEB190619594	GRB 190619B	2019-06-19T14:16:37.00	BLIND	NG	291.1	20.2	1.8	Fermi/GBM	G
HEB190620507	GRB 190620A	2019-06-20T12:10:19.50	BLIND	NG	166.2	26.8	4.4	Fermi/GBM	G
HEB190706571	GRB 190706C	2019-07-06T13:42:25.95	BLIND	NG	351.7	24.7	2.6	IPN	I
HEB190706710	GRB 190706D	2019-07-06T17:03:05.40	BLIND	NG	324.6	9.9	21.9	IPN	S
HEB190719113	GRB 190719A	2019-07-19T02:44:08.00	BLIND	NG	123.9	-30.8	5.2	Fermi/GBM	B
HEB190720964	GRB 190720B	2019-07-20T23:08:39.50	BLIND	NG	138.9	-55.6	2.3	Fermi/GBM	G
HEB190723308	GRB 190723A	2019-07-23T07:24:16.00	BLIND	NG	289.5	25.2	10.5	Fermi/GBM	G
HEB190724030	GRB 190724A	2019-07-24T00:43:56.75	BLIND	NG	170.3	15.1	13.6	Fermi/GBM	G
HEB190726642	GRB 190726A	2019-07-26T15:24:59.20	BLIND	NG	310.3	34.3	1.2	Fermi/GBM	G
HEB190806675	GRB 190806A	2019-08-06T16:12:33.32	BLIND	NG	121.1	-75.4	4.3	Fermi/GBM	G
HEB190813520	GRB 190813A	2019-08-13T12:29:09.94	BLIND	NG	106.4	-23.3	10.4	Fermi/GBM	G
HEB190814837	GRB 190814A	2019-08-14T20:05:21.00	BLIND	NG	60.4	-60.3	30.2	Fermi/GBM	G
HEB190825878	GRB 190825B	2019-08-25T21:04:54.50	BLIND	NG	-	-	-	-	B
HEB190828783	GRB 190828D	2019-08-28T18:48:33.70	BLIND	NG	251.9	-24.5	2.5	IBIS	S
HEB190831271	-	2019-08-31T06:30:27.11	BLIND	NG	-	-	-	-	S
HEB190901890	GRB 190901A	2019-09-01T21:21:57.80	BLIND	NG	230.6	-3.0	18.8	Fermi/GBM	G
HEB190903721	GRB 190903A	2019-09-03T17:19:36.26	BLIND	NG	70.5	-49.0	6.4	Fermi/GBM	G
HEB190906045	GRB 190906A	2019-09-06T01:04:50.90	BLIND	NG	267.6	-11.9	6.0	IPN	S
HEB190906767	GRB 190906B	2019-09-06T18:25:09.29	BLIND	NG	171.8	-71.6	3.5	Fermi/GBM	G
HEB190915239	GRB 190915A	2019-09-15T05:44:58.40	BLIND	NG	48.3	4.0	4.3	Fermi/GBM	G
HEB190927106	-	2019-09-27T02:33:50.30	BLIND	NG	-	-	-	-	B
HEB190928550	GRB 190928A	2019-09-28T13:12:14.00	BLIND	NG	36.6	29.5	18.4	IPN	S
HEB190928551	GRB 190928A	2019-09-28T13:13:48.40	BLIND	NG	36.6	29.5	18.4	IPN	S
HEB190929884	-	2019-09-29T21:13:49.66	BLIND	NG	-	-	-	-	B
HEB191009297	GRB 191009A	2019-10-09T07:08:56.77	BLIND	NG	29.4	63.4	9.1	Fermi/GBM	G
HEB191019970	GRB 191019B	2019-10-19T23:17:13.35	BLIND	NG	216.3	-40.6	1.0	Fermi/GBM	G
HEB191021831	-	2019-10-21T19:57:29.00	BLIND	NG	-	-	-	-	B
HEB191025779	GRB 191025B	2019-10-25T18:42:09.10	BLIND	NG	60.1	56.5	3.9	IPN	I
HEB191031182	-	2019-10-31T04:23:11.36	BLIND	NG	-	-	-	-	S
HEB191031318	GRB 191031E	2019-10-31T07:38:55.54	BLIND	NG	-	-	-	-	S

Table 3 (*continued*)

Table 3 (*continued*)

Trigger ID ^a	GRB Name	Trigger Time (UTC)	Search Method ^b	Gain Mode	RA(°)	DEC(°)	err(°)	location source ^c	Kinds of GRB samples ^d
HEB191031780	GRB 191031C	2019-10-31T18:43:16.00	BLIND	NG	115.9	-62.3	1.3	Fermi/GBM	G
HEB191105257	-	2019-11-05T06:11:08.65	BLIND	NG	297.3	24.6	3.3	Fermi/GBM	G
HEB191108003	GRB 191108A	2019-11-08T00:04:37.60	BLIND	NG	232.9	10.8	17.3	Fermi/GBM	G
HEB19111364	GRB 191111A	2019-11-11T08:44:29.95	BLIND	NG	197.2	-23.2	13.4	Fermi/GBM	G
HEB191113578	GRB 191113A	2019-11-13T13:52:44.52	BLIND	NG	298.1	20.9	5.8	Fermi/GBM	G
HEB191118925	GRB 191118A	2019-11-18T22:12:01.82	BLIND	NG	219.8	-58.7	26.8	Fermi/GBM	G
HEB191119445	-	2019-11-19T10:41:07.00	BLIND	NG	-	-	-	-	B
HEB191130506	-	2019-11-30T12:09:34.90	BLIND	NG	345.5	-4.4	14.2	Fermi/GBM	G
HEB191202378	-	2019-12-02T09:05:40.50	BLIND	NG	-	-	-	-	B
HEB191202867	GRB 191202A	2019-12-02T20:48:59.55	BLIND	NG	246.4	17.1	1.8	Fermi/GBM	G
HEB191203289	GRB 191203A	2019-12-03T06:57.19.08	BLIND	NG	332.4	51.8	34.3	Fermi/GBM	G
HEB191205740	GRB 191205A	2019-12-05T17:46:20.44	BLIND	NG	14.0	-34.1	21.4	Fermi/GBM	G
HEB191218112	GRB 191218A	2019-12-18T02:42:43.20	BLIND	NG	301.1	-40.3	0.1	Swift	G
HEB191221860	GRB 191221B	2019-12-21T20:39:10.70	BLIND	NG	154.8	-38.1	0.1	Swift	G
HEB191224829	-	2019-12-24T19:55:07.00	BLIND	NG	-	-	-	-	B
HEB191227069	GRB 191227A	2019-12-27T01:39:34.40	BLIND	NG	319.2	-16.7	0.1	Swift	G
HEB191227723	GRB 191227B	2019-12-27T17:21:44.10	BLIND	NG	258.2	-26.0	2.4	Fermi/GBM	I
HEB200109073	GRB 200109A	2020-01-09T01:45:51.89	BLIND	NG	307.1	53.0	0.1	Swift	G
HEB200111632	GRB 200111A	2020-01-11T15:11:07.61	BLIND	NG	104.5	31.7	3.5	Fermi/GBM	G
HEB200114153	GRB 200114A	2020-01-14T03:40:45.50	BLIND	NG	199.4	-0.3	2.6	Fermi/GBM	G
HEB200120961	GRB 200120A	2020-01-20T23:04:58.60	BLIND	NG	139.4	-70.7	1.0	Fermi/GBM	G
HEB200125863	GRB 200125B	2020-01-25T20:43:31.90	BLIND	NG	7.5	64.7	1.0	Fermi/GBM	G
HEB200211193	-	2020-02-11T04:38:56.10	BLIND	NG	-	-	-	-	B
HEB200219998	GRB 200219C	2020-02-19T23:57:12.05	BLIND	NG	264.5	8.4	1.0	Fermi/GBM	G
HEB200221161	GRB 200221A	2020-02-21T03:53:58.71	BLIND	NG	157.1	33.1	5.0	Fermi/GBM	G
HEB200227305	GRB 200227A	2020-02-27T07:20:16.15	BLIND	NG	56.4	9.5	0.1	Swift	G
HEB200313878	-	2020-03-13T21:04:58.00	BLIND	NG	-	-	-	-	B
HEB200323782	GRB 200323A	2020-03-23T18:46:32.80	BLIND	NG	156.5	-55.5	1.5	Fermi/GBM	G
HEB200325137	GRB 200325A	2020-03-25T03:18:31.70	BLIND	NG	22.1	-29.1	4.2	Fermi/GBM	G
HEB200326421	-	2020-03-26T10:07:36.86	BLIND	NG	-	-	-	-	S
HEB200326517	GRB 200326A	2020-03-26T12:24:47.90	BLIND	NG	245.3	-21.1	6.9	Fermi/GBM	G
HEB200412381	GRB 200412B	2020-04-12T09:08:45.80	BLIND	NG	279.8	64.1	1.0	Fermi/GBM	G
HEB200413712	-	2020-04-13T17:50:06.00	BLIND	LG	-	-	-	-	S
HEB200413743	-	2020-04-13T17:56:38.00	BLIND	NG	-	-	-	-	B
HEB200415366	GRB 200415A	2020-04-15T08:48:05.55	BLIND	NG	6.1	-32.0	2.0	Fermi/GBM	I

Table 3 *continued*

Table 3 (*continued*)

Trigger ID ^a	GRB Name	Trigger Time (UTC)	Search Method ^b	Gain Mode	RA(°)	DEC(°)	err(°)	location source ^c	Kinds of GRB samples ^d
HEB200416295	GRB 200416A	2020-04-16T07:05:17.17	BLIND	NG	335.7	-7.5	0.1	Swift	G
HEB200418864	-	2020-04-18T20:45:00.28	BLIND	NG	72.6	-1.0	-	Fermi/GBM	G
HEB200519472	GRB 200519A	2020-05-19T11:20:23.73	BLIND	NG	255.3	-30.4	0.1	Swift	G
HEB200521511	GRB 200521A	2020-05-21T12:16:41.26	BLIND	NG	169.5	7.2	4.3	IPN	S
HEB200526628	-	2020-05-26T15:04:48.31	BLIND	NG	-	-	-	-	B
HEB200601097	GRB 200601A	2020-06-01T02:19:56.50	BLIND	NG	36.7	33.5	1.7	Fermi/GBM	G
HEB200609379	GRB 200609A	2020-06-09T09:06:48.05	BLIND	NG	16.3	67.4	1.5	Fermi/GBM	G
HEB200617679	GRB 200617A	2020-06-17T16:18:05.80	BLIND	NG	359.1	-59.8	-	Fermi/GBM	G
HEB200619108	GRB 200619A	2020-06-19T02:36:11.60	BLIND	NG	101.3	56.7	4.0	Fermi/GBM	G
HEB200707072	GRB 200707A	2020-07-07T01:44:02.54	BLIND	NG	80.8	-14.9	3.1	Fermi/GBM	G
HEB200711461	GRB 200711A	2020-07-11T11:04:32.93	BLIND	NG	292.1	1.2	5.6	Fermi/GBM	G
HEB200716315	GRB 200716B	2020-07-16T07:34:29.50	BLIND	LG	350.7	-21.8	13.8	Fermi/GBM	G
HEB200716956	GRB 200716C	2020-07-16T22:57:41.18	BLIND	NG	195.6	25.1	3.5	Fermi/GBM	G
HEB200801352	GRB 200801A	2020-08-01T08:27:14.08	BLIND	NG	321.1	85.3	11.3	Fermi/GBM	G
HEB200806645	GRB 200806A	2020-08-06T15:28:49.91	BLIND	LG	52.9	37.1	0.1	Swift	G
HEB200809653	GRB 200809B	2020-08-09T15:41:27.00	BLIND	LG	359.8	-76.9	3.4	Fermi/GBM	G
HEB200824594	GRB 200824A	2020-08-24T14:15:38.82	BLIND	NG	117.7	10.5	15.4	Fermi/GBM	G
HEB200903112	GRB 200903B	2020-09-03T02:42:40.87	BLIND	NG	60.1	-13.8	14.6	Fermi/GBM	G
HEB200919964	GRB 200919C	2020-09-19T23:08:22.64	BLIND	LG	280.1	-23.7	16.8	Fermi/GBM	G
HEB200922504	GRB 200922A	2020-09-22T12:06:46.00	BLIND	NG	296.9	-55.2	0.1	Swift	G
HEB200928551	GRB 200928B	2020-09-28T13:14:44.75	BLIND	NG	85.7	2.3	17.8	Fermi/GBM	G
HEB201013157	GRB 201013A	2020-10-13T03:46:30.20	BLIND	NG	107.4	57.0	0.1	Swift	G
HEB201016019	GRB 201016A	2020-10-16T00:27:49.50	BLIND	NG	167.4	4.5	5.0	Fermi/GBM	I
HEB201105229	GRB 201105A	2020-11-05T05:31:07.76	BLIND	LG	244.5	16.0	1.0	Fermi/GBM	G
HEB201122355	GRB 201122A	2020-11-22T08:32:01.00	BLIND	NG	-	-	-	-	S
HEB201209239	GRB 201209A	2020-12-09T05:44:52.53	BLIND	NG	23.1	-1.7	0.1	Swift	G
HEB201221591	GRB 201221B	2020-12-21T14:11:43.00	BLIND	NG	110.6	32.0	4.1	Fermi/GBM	G
HEB201226553	GRB 201226A	2020-12-26T13:16:26.60	BLIND	NG	173.1	-6.0	-	Fermi/GBM	G
HEB201227634	GRB 201227A	2020-12-27T15:14:07.40	BLIND	NG	170.1	-73.6	1.5	IPN	I
HEB210112068	GRB 210112A	2021-01-12T01:38:06.55	BLIND	NG	219.0	33.1	0.1	Swift	G
HEB210119120	GRB 210119A	2021-01-19T02:54:09.82	BLIND	NG	285.8	-63.1	7.8	Fermi/GBM	G
HEB210121779	GRB 210121A	2021-01-21T18:41:48.75	BLIND	LG	17.0	-46.4	0.6	IPN	G
HEB210123304	GRB 210123A	2021-01-23T07:19:10.35	BLIND	LG	345.1	-56.9	1.1	Fermi/GBM	G
HEB210124558	GRB 210124B	2021-01-24T13:23:48.40	BLIND	LG	274.3	-0.4	0.4	IPN	S
HEB210129908	-	2021-01-29T21:48:56.90	BLIND	NG	-	-	-	-	B

Table 3 *continued*

Table 3 (*continued*)

Trigger ID ^a	GRB Name	Trigger Time (UTC)	Search Method ^b	Gain Mode	RA(°)	DEC(°)	err(°)	location source ^c	Kinds of GRB samples ^d
HEB210207911	GRB 210207B	2021-02-07T21:52:49.60	BLIND	LG	270.6	53.7	0.1	Swift IBIS	G
HEB210208564	GRB 210208A	2021-02-08T13:33:25.63	BLIND	NG	260.2	-12.7	0.1	-	S
HEB210213286	GRB 210213B	2021-02-13T06:52:27.18	BLIND	NG	-	-	-	-	S
HEB210225217	GRB 210225A	2021-02-25T05:13:36.00	BLIND	NG	333.4	28.4	3.4	Fermi/GBM	G
HEB210227114	-	2021-02-27T02:45:09.42	BLIND	NG	115.8	61.1	-	Fermi/GBM	G
HEB210228057	GRB 210228B	2021-02-28T01:22:53.90	BLIND	NG	283.5	-43.1	-	Fermi/GBM	G
HEB210306320	-	2021-03-06T07:41:07.50	BLIND	NG	-	-	-	-	B
HEB210306879	-	2021-03-06T21:07:09.56	BLIND	NG	-	-	-	-	B
HEB210307247	GRB 210307B	2021-03-07T05:56:37.94	BLIND	LG	125.6	17.5	7.3	GECAM	G
HEB210323918	GRB 210323A	2021-03-23T22:02:18.40	BLIND	NG	317.9	25.4	0.1	Swift	G
HEB210324468	-	2021-03-24T11:14:28.21	BLIND	NG	148.5	37.2	-	Fermi/GBM	G
HEB210326057	GRB 210326A	2021-03-26T01:22:24.93	BLIND	NG	58.0	15.1	39.2	Fermi/GBM	G
HEB210326890	-	2021-03-26T21:22:24.93	BLIND	NG	-	-	-	-	B
HEB210328396	-	2021-03-28T09:30:52.77	BLIND	NG	-	-	-	-	B
HEB210405507	-	2021-04-05T12:11:26.68	BLIND	NG	-	-	-	-	B
HEB210406716	GRB 210406A	2021-04-06T17:11:28.92	BLIND	NG	132.5	76.5	0.1	IBIS	S
HEB210409894	GRB 210409A	2021-04-09T21:28:26.86	BLIND	NG	70.9	-58.3	2.9	GECAM	G
HEB210411147	GRB 210411A	2021-04-11T03:31:41.10	BLIND	NG	259.4	-27.4	3.0	Fermi/GBM	G
HEB210421454	GRB 210421B	2021-04-21T10:54:44.81	BLIND	NG	272.1	57.2	2.1	Fermi/GBM	G
HEB210422572	GRB 210422B	2021-04-22T13:44:37.13	BLIND	NG	116.6	24.7	2.1	Fermi/GBM	G
HEB210427206	GRB 210427A	2021-04-27T04:57:12.99	BLIND	NG	177.3	-53.4	1.1	Fermi/GBM	G
HEB210429071	-	2021-04-29T01:43:11.33	BLIND	NG	-	-	-	-	B
HEB210502295	-	2021-05-02T07:05:16.38	BLIND	NG	-	-	-	-	B
HEB210504958	-	2021-05-04T23:00:47.17	BLIND	NG	-	-	-	-	B
HEB210506027	GRB 210506A	2021-05-06T00:39:48.54	BLIND	LG	224.2	-32.7	43.0	IPN	B
HEB210511476	GRB 210511B	2021-05-11T11:26:39.26	BLIND	NG	316.2	61.7	1.0	Fermi/GBM	G
HEB210511647	-	2021-05-11T15:32:56.10	BLIND	NG	-	-	-	-	B
HEB210515546	GRB 210515A	2021-05-15T13:06:45.70	BLIND	NG	117.1	77.3	14.6	Fermi/GBM	G
HEB210516982	GRB 210516A	2021-05-16T23:34:45.86	BLIND	NG	22.1	74.9	9.5	Fermi/GBM	G
HEB210518544	GRB 210518A	2021-05-18T13:04:09.64	BLIND	NG	270.0	49.6	1.8	Fermi/GBM	G
HEB210520796	GRB 210520A	2021-05-20T19:07:02.00	BLIND	NG	147.9	-67.0	3.7	Fermi/GBM	G
HEB210602502	GRB 210602A	2021-06-02T12:04:01.32	BLIND	LG	44.6	-2.7	0.2	MAXI/GSC	S
HEB210605214	GRB 210605A	2021-06-05T05:08:58.39	BLIND	NG	21.7	-41.5	2.0	Fermi/GBM	G
HEB210606120	-	2021-06-06T02:53:02.89	BLIND	NG	-	-	-	-	B
HEB210606945	GRB 210606B	2021-06-06T22:41:05.24	BLIND	NG	87.5	-18.4	1.2	Fermi/GBM	G

Table 3 continued

Table 3 (*continued*)

Trigger ID ^a	GRB Name	Trigger Time (UTC)	Search Method ^b	Gain Mode	RA(°)	DEC(°)	err(°)	location source ^c	Kinds of GRB samples ^d
HEB210607775	GRB 210607B	2021-06-07T18:37:17.80	BLIND	NG	-	-	-	-	B
HEB210607902	GRB 210607C	2021-06-07T21:39:20.72	BLIND	NG	-	-	-	-	B
HEB210610827	GRB 210610B	2021-06-10T19:51:05.05	BLIND	NG	243.9	14.4	0.1	Swift	G
HEB210615891	-	2021-06-15T21:23:51.50	BLIND	NG	-	-	-	-	B
HEB210615981	GRB 210615A	2021-06-15T23:33:53.60	BLIND	NG	342.9	62.2	7.5	Fermi/GBM	G
HEB210622064	GRB 210622A	2021-06-22T01:32:35.94	BLIND	NG	242.1	-14.1	6.1	Fermi/GBM	G
HEB210622339	-	2021-06-22T08:09:30.61	BLIND	NG	-	-	-	-	B
HEB210627311	GRB 210627A	2021-06-27T07:29:15.68	BLIND	NG	148.3	44.5	10.7	Fermi/GBM	G
HEB210627813	-	2021-06-27T19:31:37.68	BLIND	NG	-	-	-	-	B

*a*The trigger ID starts with a ‘HEB’ label which means ‘HE-detected Burst’.

b As clarified in Sec 3, BLIND: blind search, TARGETED: targeted search.

c The uncertainties of the locations from *Swift*/BAT are 90% containment, including systematic uncertainty, while those from *Fermi*/GBM and other detections are 1σ containment, statistical only. If the location source is from interplanetary network (IPN) triangulation, the error is determined to be the maximum dimension of error box area. Instrument detections are defined as: Fermi/LAT: Large Area Telescope, IBIS: Imager on Board Integral Satellite in INTEGRAL.

d As shown in Table 2, G: GOLDEN, S: SILVER, B: BRONZE, I: IRON.

Table 4. Durations (10–2000 keV) from joint analyses with ‘GOLDEN’ GRB samples.

Trigger ID	Detectors Used	T_{50} (s)	T_{50} start (s)	T_{90} (s)	T_{90} start (s)	T_{90} only with HXMT/CsI counts (s)
HEB170626400	HXMT/CsI, Fermi-GBM (n0, n1, n2, b0)	7.040±0.264	1.248	12.416±0.202	0.224	12.690±0.081
HEB170705115	HXMT/CsI, Fermi-GBM (n8, nb, b1)	33.792±3.714	0.496	68.672±1.601	-6.416	18.460±6.340
HEB170714049	HXMT/CsI, Fermi-GBM (n3, n7, b0, b1)	0.128±0.064	-0.156	0.448±0.143	-0.412	0.835±0.220
HEB170718152	HXMT/CsI, Fermi-GBM (n3, n4, b0)	10.624±1.943	-7.144	24.768±3.562	-13.352	24.160±3.322
HEB170726248	HXMT/CsI, Fermi-GBM (n9, n7)	1.344±0.143	-0.232	5.824±1.537	-1.704	2.580±0.061
HEB170726793	HXMT/CsI, Fermi-GBM (n8, n7, b1)	10.432±0.272	1.364	26.240±2.689	-5.612	22.871±0.901
HEB170728960	HXMT/CsI, Fermi-GBM (n6, n9, b1)	12.864±0.202	0.684	19.840±0.962	0.364	16.860±2.371
HEB170731751	HXMT/CsI, Fermi-GBM (n0, n3, b0)	41.664±1.604	4.336	59.584±3.623	-2.768	28.141±6.360
HEB170802637	HXMT/CsI, Fermi-GBM (n6, n8, b1)	0.192±0.091	0.696	2.176±1.793	-1.288	0.820±0.014
HEB170817908	HXMT/CsI, Fermi-GBM (n0, n1, n2, n5, b0)	1.472±0.143	0.544	2.688±0.202	0.288	2.620±0.081
HEB170825306	HXMT/CsI, Fermi-GBM (n3, n7, b0, b1)	3.328±0.181	-0.713	11.712±2.244	-2.441	7.340±1.872
HEB170826818	HXMT/CsI, Fermi-GBM (n4, nb, b1)	5.952±0.091	1.424	11.392±0.264	-0.432	9.537±0.161
HEB170903534	HXMT/CsI, Fermi-GBM (n4, n8, b0, b1)	11.328±1.414	-2.502	26.048±1.414	-6.022	19.050±3.960
HEB170906029	HXMT/CsI, Fermi-GBM (n4, n3, b0)	38.912±0.466	31.724	93.120±1.294	8.556	63.610±2.140
HEB170912984	HXMT/CsI, Fermi-GBM (n7, n8, b1)	1.728±1.154	-1.680	2.880±0.834	-2.256	4.005±0.708
HEB170923188	HXMT/CsI, Fermi-GBM (n4, n7, b0)	12.672±2.636	9.533	32.960±2.561	-0.451	25.660±1.310
HEB171008079	HXMT/CsI, Fermi-GBM (n4, n8, b0, b1)	5.248±0.326	0.352	12.672±3.721	-2.976	1.169±1.819
HEB171013350	HXMT/CsI, Fermi-GBM (n2, n3, b0)	13.312±0.345	6.296	32.000±0.771	-2.920	22.710±5.620
HEB171020963	HXMT/CsI, Swift/BAT	6.400±1.231	-2.416	10.176±0.091	-5.040	9.620±2.070
HEB171030728	HXMT/CsI, Fermi-GBM (n7, n8, b1)	0.320±0.453	0.052	1.344±0.643	-0.716	0.475±1.481
HEB171103965	HXMT/CsI, Swift/BAT	0.064±0.091	2.032	0.192±0.091	1.968	0.197±0.022
HEB171120555	HXMT/CsI, Fermi-GBM (n0, n3, b0)	39.488±0.143	1.312	52.160±1.601	0.480	43.461±9.610
HEB171124234	HXMT/CsI, Fermi-GBM (n0, n3, b0)	5.312±0.362	-3.608	18.112±0.653	-6.424	6.197±0.490
HEB171207054	HXMT/CsI, Fermi-GBM (n0, n1, b0)	0.192±0.091	-0.104	4.864±2.625	-1.320	3.010±0.358
HEB171209615	HXMT/CsI, Swift/BAT	61.376±1.358	11.792	93.696±2.567	-0.944	84.781±10.092
HEB171210492	HXMT/CsI, Fermi-GBM (n9, n1, b0, b1)	48.128±1.414	7.544	108.224±3.137	1.592	15.950±1.773
HEB171215705	HXMT/CsI, Fermi-GBM (n8, nb, b1)	13.696±1.096	0.672	34.496±8.192	-4.576	32.016±8.414

Table 4 continued

Table 4 (*continued*)

Trigger ID	Detectors Used	T_{50} (s)	T_{50} start (s)	T_{90} (s)	T_{90} start (s)	T_{90} only with HXMT/CsI counts (s)
HEB171223818	HXMT/CsI, Fermi-GBM (n7, n6, b1)	1.088±0.219	0.632	1.216±0.219	0.632	0.160±0.014
HEB171230955	HXMT/CsI, Fermi-GBM (n7, n8, b1)	24.768±1.105	6.056	77.440±4.636	-1.368	20.050±2.241
HEB180110608	HXMT/CsI, Fermi-GBM (n7, n9, b1)	7.488±3.393	-0.712	13.952±0.580	-4.424	14.290±2.930
HEB180111695	HXMT/CsI, Swift/BAT	9.920±0.091	2.604	27.008±3.073	0.108	21.040±6.820
HEB180119836	HXMT/CsI, Fermi-GBM (n0, n1, b0)	2.112±0.202	2.800	6.144±1.802	0.176	9.380±3.110
HEB180127049	HXMT/CsI, Fermi-GBM (n3, n7, b0, b1)	7.744±0.345	2.400	21.312±1.541	-2.400	22.669±1.377
HEB180130744	HXMT/CsI, Fermi-GBM (n6, n8, b1)	0.064±0.264	-0.148	1.280±1.154	-0.148	1.997±0.516
HEB180208764	HXMT/CsI, Fermi-GBM (na, nb, b1)	4.544±0.547	-1.896	27.328±1.856	-15.976	5.603±0.283
HEB180210517	HXMT/CsI, Fermi-GBM (n0, n1, b0)	16.704±0.181	6.104	40.448±0.707	-1.384	17.028±1.415
HEB180305393	HXMT/CsI, Fermi-GBM (m9, na, b1)	4.096±0.091	3.768	10.944±0.453	1.464	4.002±0.283
HEB180306972	HXMT/CsI, Fermi-GBM (n3, n5, b0)	9.984±1.431	0.928	33.856±9.605	-3.232	26.303±12.649
HEB180309321	HXMT/CsI, Fermi-GBM (n7, n8, b1)	16.832±1.694	5.344	44.608±2.248	-1.504	50.456±5.352
HEB180313977	HXMT/CsI, Fermi-GBM (m0, n1, b0)	0.064±0.389	-0.008	0.832±0.453	-0.008	1.201±0.283
HEB180330891	HXMT/CsI, Fermi-GBM (n1, n3, b0)	4.800±0.580	1.168	15.168±1.282	0.144	5.860±1.180
HEB180331177	HXMT/CsI, Swift/BAT	16.320±1.350	1.232	29.563±2.499	-4.272	35.780±9.670
HEB180401279	HXMT/CsI, Fermi-GBM (n2, na, b0, b1)	6.208±0.231	2.112	13.952±0.462	-1.600	6.003±0.283
HEB180402406	HXMT/CsI, Fermi-GBM (n6, n8, b1)	0.128±0.091	-0.048	0.384±0.326	-0.304	0.411±0.007
HEB180404091	HXMT/CsI, Fermi-GBM (n3, n4, b0)	17.088±1.421	7.119	59.904±3.267	0.783	53.141±8.120
HEB180409346	HXMT/CsI, Fermi-GBM (n9, b1)	6.912±0.091	4.616	12.864±0.264	1.288	11.510±0.530
HEB180413117	HXMT/CsI, Fermi-GBM (n6, n7, b1)	21.760±1.002	0.304	84.352±7.059	-25.296	21.010±5.206
HEB180416923	HXMT/CsI, Fermi-GBM (n4, n7, b0, b1)	28.352±1.860	3.896	74.816±1.473	0.376	27.250±2.330
HEB180427442	HXMT/CsI, Fermi-GBM (n6, n4, b0, b1)	9.280±0.202	3.952	29.824±1.218	0.816	7.240±0.311
HEB180505539	HXMT/CsI, Fermi-GBM (n8, n4, b0, b1)	4.224±0.091	-3.032	28.096±1.159	-20.376	27.751±9.580
HEB180506902	HXMT/CsI, Fermi-GBM (n2, n5, b0, b1)	13.888±0.528	1.504	21.760±0.905	-2.720	17.409±6.280
HEB180510808	HXMT/CsI, Swift/BAT	2.752±0.091	0.688	39.744±4.224	-9.296	20.526±8.569
HEB180523782	HXMT/CsI, Fermi-GBM (n0, n1, b0)	1.728±0.547	-0.968	7.936±1.118	-3.720	6.702±4.189
HEB180525151	HXMT/CsI, Fermi-GBM (n4, n5, b0, b1)	0.064±0.091	0.012	0.320±0.264	-0.052	0.361±0.076
HEB180605457	HXMT/CsI, Fermi-GBM (n0, n2, b0)	9.408±0.202	4.256	22.784±1.601	0.736	17.670±0.670
HEB180618030	HXMT/CsI, Fermi-GBM (n4, n5, b0, b1)	0.576±0.143	-0.288	5.056±0.716	-3.488	3.501±0.855
HEB180623696	HXMT/CsI, Swift/BAT	18.624±2.057	-6.976	64.768±0.453	-24.960	64.811±3.820

Table 4 *continued*

Table 4 (*continued*)

Trigger ID	Detectors Used	T_{50} (s)	T_{50} start (s)	T_{90} (s)	T_{90} start (s)	T_{90} only with HXMT/CsI counts (s)
HEB180625940	HXMT/CsI, Fermi-GBM (n4, n8, b0)	0.256±0.091	0.120	2.048±0.962	-0.776	0.310±0.071
HEB180626391	HXMT/CsI, Fermi-GBM (n9, na, b1)	0.320±0.091	-0.340	0.768±0.453	-0.340	0.770±0.070
HEB180704233	HXMT/CsI, Swift/BAT	18.368±0.320	-18.880	32.384±1.833	-28.992	20.030±1.414
HEB180715754	HXMT/CsI, Fermi-GBM (n9, na, b1)	0.448±0.091	-0.004	1.280±0.870	-0.580	0.640±0.175
HEB180718762	HXMT/CsI, Fermi-GBM (n0, n2, b0)	23.232±1.231	6.312	59.776±3.142	1.512	21.550±0.500
HEB180722992	HXMT/CsI, Fermi-GBM (n2, n1, b0)	41.920±0.975	13.312	116.800±4.740	1.024	90.122±0.689
HEB180724807	HXMT/CsI, Fermi-GBM (na, nb, b1)	17.792±0.590	6.584	52.224±1.921	1.400	53.066±14.026
HEB180730017	HXMT/CsI, Fermi-GBM (n4, n5, b0)	0.000±0.962	0.312	1.664±1.601	0.248	0.100±1.561
HEB180801275	HXMT/CsI, Fermi-GBM (n6, n7, b1)	0.192±0.091	-0.008	0.704±0.264	-0.456	0.550±0.114
HEB180803590	HXMT/CsI, Fermi-GBM (n3, n4, b0)	0.128±0.091	-0.240	0.256±0.516	-0.304	0.350±0.071
HEB180804930	HXMT/CsI, Fermi-GBM (n8, nb, b1)	5.824±0.771	0.496	23.040±1.802	-3.472	4.620±0.240
HEB180816088	HXMT/CsI, Fermi-GBM (n2, n1, b0)	15.040±0.320	9.015	39.168±2.180	-0.137	59.074±5.031
HEB180822561	HXMT/CsI, Fermi-GBM (m0, n1, b0)	2.816±0.286	-0.344	13.568±2.463	-3.480	4.506±1.119
HEB180828789	HXMT/CsI, Fermi-GBM (n9, na, b1)	4.032±0.091	4.512	8.448±0.143	1.440	7.750±0.122
HEB180925407	HXMT/CsI, Fermi-GBM (n4, n5, b0)	2.496±0.405	-2.952	5.440±2.308	-4.808	5.601±1.360
HEB180925609	HXMT/CsI, Swift/BAT	13.312±0.286	3.304	33.664±1.484	-5.080	10.640±0.940
HEB180927992	HXMT/CsI, Fermi-GBM (n1, n5, b0)	3.392±0.590	-0.264	11.584±2.753	-2.568	3.380±0.256
HEB180929453	HXMT/CsI, Fermi-GBM (n1, n2, b0)	2.368±0.091	-0.008	3.008±0.143	-0.264	2.850±0.190
HEB181008269	HXMT/CsI, Fermi-GBM (n9, na, b1)	11.264±0.362	-3.384	49.920±3.014	-24.312	31.039±1.583
HEB181014479	HXMT/CsI, Fermi-GBM (n1, n4, b0)	8.128±0.405	-4.248	25.728±2.755	-9.432	23.507±3.042
HEB181028590	HXMT/CsI, Fermi-GBM (n7, n8, b1)	14.784±0.429	9.360	33.088±1.358	1.040	29.061±3.021
HEB181119605	HXMT/CsI, Fermi-GBM (n7, n9, b1)	8.960±0.181	5.714	18.432±0.389	0.146	15.090±0.871
HEB181121306	HXMT/CsI, Fermi-GBM (n8, b1)	0.384±0.326	-0.240	0.576±0.143	-0.304	0.621±0.822
HEB181122381	HXMT/CsI, Fermi-GBM (n7, n8, b1)	15.232±1.645	4.872	40.768±7.040	0.136	21.491±5.498
HEB181123231	HXMT/CsI, Swift/BAT	0.128±0.090	0.090	0.256±0.090	0.024	0.370±0.330
HEB181212692	HXMT/CsI, Fermi-GBM (n2, n5, b0)	8.768±1.218	2.512	58.752±3.585	0.848	47.059±7.509
HEB181213540	HXMT/CsI, Swift/BAT	11.392±0.905	2.592	22.720±2.177	0.480	21.527±3.540
HEB181217664	HXMT/CsI, Fermi-GBM (n2, na, b0)	8.256±0.389	11.440	33.088±4.100	2.736	25.630±2.580
HEB181225489	HXMT/CsI, Fermi-GBM (n3, n7, b0)	9.344±0.264	1.312	35.776±2.817	0.672	10.110±0.440
HEB190103877	HXMT/CsI, Swift/BAT	9.856±0.345	1.440	24.448±3.216	-7.776	10.202±0.224

Table 4 *continued*

Table 4 (*continued*)

Trigger ID	Detectors Used	T_{50} (s)	T_{50} start (s)	T_{90} (s)	T_{90} start (s)	T_{90} only with HXMT/CsI counts (s)
HEB190110725	HXMT/CsI, Fermi-GBM (n3, n5, b0, b1)	3.456±0.181	-2.536	11.904±2.244	-5.096	6.838±1.085
HEB190131964	HXMT/CsI, Fermi-GBM (n9, na, b1)	12.800±0.859	4.136	36.544±5.824	0.744	23.620±1.290
HEB190215771	HXMT/CsI, Fermi-GBM (m1, n3, b0)	8.064±0.326	3.896	25.216±2.369	0.760	15.010±2.470
HEB190222537	HXMT/CsI, Fermi-GBM (n9, nb, b1)	6.208±0.516	1.448	28.992±3.009	-0.088	4.802±0.633
HEB190226515	HXMT/CsI, Fermi-GBM (n9, na, b1)	0.064±0.091	0.160	0.192±0.389	0.096	0.470±0.125
HEB190310398	HXMT/CsI, Fermi-GBM (n3, n5, b0, b1)	6.720±0.143	-1.696	75.072±1.537	-51.680	64.080±27.038
HEB190324348	HXMT/CsI, Fermi-GBM (n1, na, b0, b1)	16.896±1.541	3.456	51.136±1.569	-1.152	49.562±4.036
HEB190324947	HXMT/CsI, Fermi-GBM (n6, n7, b1)	5.056±0.202	1.664	12.736±0.580	-0.256	6.700±0.501
HEB190326313	HXMT/CsI, Fermi-GBM (n0, n3, b0)	25.792±4.740	22.749	68.160±5.874	-5.283	60.111±12.830
HEB190326316	HXMT/CsI, Swift/BAT	0.064±0.389	-0.040	0.576±0.429	-0.232	0.325±0.011
HEB190330694	HXMT/CsI, Fermi-GBM (n1, n9, b0)	23.808±1.409	1.648	45.760±2.113	0.432	8.080±0.860
HEB190331093	HXMT/CsI, Fermi-GBM (n0, n3)	18.176±2.147	-15.728	35.008±2.947	-24.496	18.022±1.805
HEB190401139	HXMT/CsI, Fermi-GBM (n6, n7, b1)	10.944±0.326	3.568	31.104±1.154	0.112	21.020±3.900
HEB190407671	HXMT/CsI, Fermi-GBM (n8, n9, b1)	6.848±0.264	1.136	14.400±0.643	-1.808	4.506±0.707
HEB190422283	HXMT/CsI, Fermi-GBM (n4, n8, b0)	61.312±0.590	13.288	86.976±1.620	-1.624	64.321±6.352
HEB190424417	HXMT/CsI, Swift/BAT	12.928±0.405	1.000	31.040±2.180	-2.904	23.410±4.840
HEB190507269	HXMT/CsI, Fermi-GBM (n9, na, b1)	7.488±0.716	0.761	18.560±1.282	-1.159	12.180±3.861
HEB190515189	HXMT/CsI, Fermi-GBM (n6, n9, b1)	0.192±0.091	0.160	0.448±0.091	0.032	0.400±0.087
HEB190525031	HXMT/CsI, Fermi-GBM (na, n9, b1)	0.512±0.091	0.064	1.344±0.516	-0.064	1.750±0.757
HEB190531840	HXMT/CsI, Fermi-GBM (n0, n3, b0)	13.632±0.091	18.360	37.248±4.224	7.544	29.390±1.400
HEB190604446	HXMT/CsI, Fermi-GBM (n4, n3, b0)	4.480±0.143	3.052	13.184±0.834	0.044	9.902±2.721
HEB190613449	HXMT/CsI, Fermi-GBM (n7, n8, b1)	1.408±0.143	0.880	2.816±0.264	0.112	2.340±0.022
HEB190615636	HXMT/CsI, Fermi-GBM (nb, n8, b1)	8.256±0.373	0.736	21.888±1.132	-8.480	8.820±0.780
HEB190619594	HXMT/CsI, Fermi-GBM (nb, n7, b1)	70.080±1.874	4.768	136.128±5.089	-8.736	131.664±22.033
HEB190620507	HXMT/CsI, Fermi-GBM (n3, n4, b0)	16.320±0.834	3.824	55.936±1.275	-2.896	54.568±1.805
HEB190720964	HXMT/CsI, Fermi-GBM (n3, n4, b0)	3.264±0.326	0.173	11.520±2.305	-1.171	7.509±1.583
HEB190723308	HXMT/CsI, Fermi-GBM (n7, n8, b1)	16.640±0.643	0.848	27.136±3.841	-4.144	18.022±2.064
HEB190724030	HXMT/CsI, Fermi-GBM (n0, n5, b1)	0.064±0.091	-0.004	0.192±0.143	-0.132	0.430±0.032
HEB190726642	HXMT/CsI, Fermi-GBM (n9, na, b1)	4.096±0.202	-1.576	17.472±1.958	-7.144	4.570±0.530
HEB190806675	HXMT/CsI, Fermi-GBM (n0, n1, b0)	8.960±0.429	2.241	24.384±3.585	-0.063	16.020±0.708

Table 4 *continued*

Table 4 (continued)

Trigger ID	Detectors Used	T_{50} (s)	T_{50} start (s)	T_{90} (s)	T_{90} start (s)	T_{90} only with HXMT/CsI counts (s)
HEB190813520	HXMT/CsI, Fermi-GBM (n2, n9, b0)	0.064±0.143	-0.072	0.640±0.771	-0.072	1.200±0.022
HEB190814837	HXMT/CsI, Fermi-GBM (nb, n9, b1)	4.928±0.653	0.485	13.184±3.009	-3.035	5.910±0.430
HEB190901890	HXMT/CsI, Fermi-GBM (n3, n4, b0)	7.872±0.202	0.656	23.360±1.096	-5.808	16.620±3.221
HEB190903721	HXMT/CsI, Fermi-GBM (n7, n8, b1)	0.192±0.091	-0.212	0.320±0.389	-0.276	0.450±0.461
HEB190906767	HXMT/CsI, Fermi-GBM (n4, n8, b0)	23.424±0.643	0.440	38.336±2.497	-0.072	16.710±4.870
HEB190915239	HXMT/CsI, Fermi-GBM (nb, n8, b1)	6.656±0.590	1.064	15.488±0.854	-1.432	7.230±0.830
HEB191009297	HXMT/CsI, Fermi-GBM (n9, b1)	48.192±6.977	7.400	88.128±3.992	0.424	53.566±18.050
HEB191019970	HXMT/CsI, Fermi-GBM (n0, n5, b0, b1)	104.256±0.692	22.991	142.976±2.636	7.311	136.833±16.050
HEB191031780	HXMT/CsI, Fermi-GBM (n0, n6, b0, b1)	21.952±0.516	26.159	75.264±6.849	0.623	49.951±4.510
HEB191105257	HXMT/CsI, Fermi-GBM (n4, n8)	0.064±0.091	0.024	0.192±0.091	-0.040	0.145±0.007
HEB191108003	HXMT/CsI, Fermi-GBM (n0, n1, b0)	94.784±2.273	19.596	164.736±7.700	-3.572	116.579±16.204
HEB191111364	HXMT/CsI, Fermi-GBM (n4, n0)	33.216±0.659	26.808	99.264±0.668	-6.280	96.016±17.567
HEB191113578	HXMT/CsI, Fermi-GBM (n4, n8, b0)	10.432±3.521	0.672	19.008±0.834	0.160	24.530±4.615
HEB1911118925	HXMT/CsI, Fermi-GBM (n2, n5, b0)	13.824±1.793	6.520	75.968±7.745	1.080	15.390±1.760
HEB191130506	HXMT/CsI, Fermi-GBM (n0, n9, b0, b1)	17.024±0.854	3.304	46.720±5.422	-0.664	46.057±10.025
HEB191202867	HXMT/CsI, Fermi-GBM (m0, n3, b0)	6.656±0.462	-2.008	33.408±2.499	-7.768	4.180±1.145
HEB191203289	HXMT/CsI, Fermi-GBM (n0, n1, b0)	0.192±0.091	-0.338	0.448±0.516	-0.466	0.695±0.276
HEB191205740	HXMT/CsI, Fermi-GBM (n3, n4, b0)	2.496±0.466	-3.892	3.840±0.962	-4.084	3.920±0.581
HEB191218112	HXMT/CsI, Swift/BAT	41.664±0.345	3.112	53.824±2.689	-0.216	49.811±1.240
HEB191221860	HXMT/CsI, Swift/BAT	4.096±0.091	1.944	13.632±0.962	-1.960	13.016±1.119
HEB191227069	HXMT/CsI, Fermi-GBM (n2, n1, b0)	8.256±0.202	0.808	28.032±1.562	-6.872	24.030±1.583
HEB200109073	HXMT/CsI, Fermi-GBM (n5, n2, b0)	24.704±1.489	2.720	40.256±1.869	-4.512	25.540±5.260
HEB200111632	HXMT/CsI, Fermi-GBM (n9, na, b1)	5.184±0.091	0.760	10.240±1.665	-3.528	11.500±2.501
HEB200114153	HXMT/CsI, Fermi-GBM (n2, na, b0, b1)	26.048±0.590	0.304	42.496±6.529	-2.512	28.035±5.105
HEB200120961	HXMT/CsI, Fermi-GBM (n6, na, b1)	4.160±0.231	-2.700	14.400±2.369	-6.732	14.660±1.354
HEB200125863	HXMT/CsI, Fermi-GBM (n0, n1, b0, b1)	2.624±0.091	0.888	6.400±0.202	-0.072	4.240±0.330
HEB200219998	HXMT/CsI, Fermi-GBM (m0, n1, b0)	9.920±0.707	0.744	22.784±0.580	-0.920	3.760±3.660
HEB200221161	HXMT/CsI, Fermi-GBM (n8, nb, b1)	0.512±0.143	-0.264	8.128±0.771	-4.616	1.460±0.121
HEB200227305	HXMT/CsI, Fermi-GBM (m0, n1, b0)	7.936±0.286	-1.072	23.488±2.627	-7.536	19.450±2.240
HEB200323782	HXMT/CsI, Fermi-GBM (m7, n9, b1)	0.768±0.091	0.440	1.664±0.264	0.056	1.601±0.141

Table 4 continued

Table 4 (*continued*)

Trigger ID	Detectors Used	T_{50} (s)	T_{50} start (s)	T_{90} (s)	T_{90} start (s)	T_{90} only with HXMT/CsI counts (s)
HEB200325137	HXMT/CsI, Fermi-GBM (n3, n5, b0)	0.576±0.143	0.120	1.728±1.154	-0.008	1.210±0.014
HEB200326517	HXMT/CsI, Fermi-GBM (n9, nb, b1)	1.728±0.405	-0.636	2.816±1.032	-1.020	2.410±1.131
HEB200412381	HXMT/CsI, Fermi-GBM (n6, n8, b1)	1.920±0.091	2.820	7.616±0.389	-0.444	6.360±0.139
HEB200416295	HXMT/CsI, Fermi-GBM (n2, n5)	3.328±0.264	0.160	7.616±1.473	-1.888	6.310±2.181
HEB200418864	HXMT/CsI, Fermi-GBM (n3, n4, b0)	15.360±4.420	5.736	38.080±3.905	0.680	12.900±8.113
HEB200519472	HXMT/CsI, Swift/BAT	5.760±0.604	21.168	32.832±2.052	8.560	30.890±2.520
HEB200601097	HXMT/CsI, Fermi-GBM (n1, n5, b0)	119.296±0.716	12.512	158.144±4.612	-3.104	10.570±8.741
HEB200609379	HXMT/CsI, Fermi-GBM (n0, n4, b0)	27.584±1.319	2.576	93.248±3.912	-44.400	88.071±8.960
HEB200617679	HXMT/CsI, Fermi-GBM (n8, n4, b0)	0.192±0.091	-0.136	1.024±1.729	-0.776	0.910±0.028
HEB200619108	HXMT/CsI, Fermi-GBM (n5, n4, b0)	8.640±0.607	1.532	28.672±6.528	0.188	27.534±7.027
HEB200707072	HXMT/CsI, Fermi-GBM (n3, n1)	7.360±1.368	3.128	20.224±2.191	-0.776	16.521±6.028
HEB200711461	HXMT/CsI, Fermi-GBM (n7, n9, b1)	14.720±0.580	3.560	29.376±1.478	0.488	12.190±6.180
HEB200716315	HXMT/CsI, Fermi-GBM (n6, n7, b1)	22.528±0.968	2.000	43.968±2.241	-0.624	42.053±13.026
HEB200716956	HXMT/CsI, Fermi-GBM (n0, n1, b0)	1.920±0.091	0.320	4.416±0.707	0.192	2.140±0.014
HEB200801352	HXMT/CsI, Fermi-GBM (n6, n8)	16.320±2.360	-3.288	34.240±4.394	-10.072	24.470±4.150
HEB200806645	HXMT/CsI, Swift/BAT	10.816±0.429	15.312	37.376±5.130	0.848	33.050±2.060
HEB200809653	HXMT/CsI, Fermi-GBM (n7, n8, b1)	5.120±0.707	0.280	14.656±3.334	-1.000	17.522±2.553
HEB200824594	HXMT/CsI, Fermi-GBM (n0, n3)	0.320±0.834	-0.456	1.664±0.707	-0.840	0.850±0.112
HEB200903112	HXMT/CsI, Fermi-GBM (n7, b1)	38.528±2.589	4.056	89.152±3.917	-16.424	40.026±2.809
HEB200919964	HXMT/CsI, Fermi-GBM (n7, n8, b1)	36.224±0.716	11.152	57.280±1.444	1.680	58.261±7.300
HEB200922504	HXMT/CsI, Swift/BAT	7.552±1.096	0.504	16.512±1.118	-2.760	4.440±1.192
HEB200928551	HXMT/CsI, Fermi-GBM (n9, na, b1)	7.872±0.231	-2.720	19.584±2.627	-6.112	15.160±1.990
HEB201013157	HXMT/CsI, Swift/BAT	1.856±0.326	0.560	6.912±0.202	0.048	2.010±0.022
HEB201105229	HXMT/CsI, Fermi-GBM (n3, n5, b0)	5.184±0.202	2.744	16.384±1.282	0.952	12.010±0.960
HEB201209239	HXMT/CsI, Swift/BAT	14.976±2.988	-7.104	45.632±1.843	-24.064	12.370±0.466
HEB201221591	HXMT/CsI, Fermi-GBM (na, nb)	0.010±0.014	0.048	0.050±0.045	0.038	0.035±0.007
HEB201226553	HXMT/CsI, Fermi-GBM (n2, na)	52.544±1.088	8.464	71.360±0.842	-1.584	71.022±5.270
HEB210112068	HXMT/CsI, Swift/BAT	6.784±0.143	1.792	96.512±0.771	-58.496	12.500±2.060
HEB210119120	HXMT/CsI, Fermi-GBM (n1, n3, b0)	0.032±0.091	-0.032	0.064±0.091	-0.032	0.060±0.061
HEB210121779	HXMT/CsI, Fermi-GBM (n0, n3, b0)	7.040±0.453	1.528	15.424±0.643	0.312	13.980±0.170

Table 4 *continued*

Table 4 (continued)

Trigger ID	Detectors Used	T_{50} (s)	T_{50} start (s)	T_{90} (s)	T_{90} start (s)	T_{90} only with HXMT/CsI counts (s)
HEB210123304	HXMT/CsI, Fermi-GBM (n2, n5, b0)	5.888±0.231	-2.928	15.488±1.282	-6.896	12.330±0.990
HEB210207911	HXMT/CsI, Swift/BAT	27.968±0.202	-26.192	43.584±0.389	-40.400	42.501±0.631
HEB210225217	HXMT/CsI, Fermi-GBM (n1, n5, b0)	6.720±0.286	1.432	19.392±4.615	-1.000	10.100±3.340
HEB210227114	HXMT/CsI, Fermi-GBM (n9, n6, b1)	10.880±1.833	4.664	25.088±1.409	1.272	10.704±1.903
HEB210228057	HXMT/CsI, Fermi-GBM (n4, n5, b0)	0.640±0.091	0.056	1.408±0.516	-0.200	1.620±0.370
HEB210307247	HXMT/CsI, GECAM	0.896±0.091	0.216	1.216±0.771	-0.040	0.190±0.014
HEB210323918	HXMT/CsI, Fermi-GBM (n0, n1, n2, n5, b0)	0.128±0.091	-0.008	0.832±0.453	-0.392	1.240±0.990
HEB210324468	HXMT/CsI, Fermi-GBM (n7, n8, b1)	16.768±0.362	4.448	34.432±1.282	-3.808	33.109±10.330
HEB210326057	HXMT/CsI, Fermi-GBM (n4, n5, b0)	0.128±0.143	-0.080	1.024±0.923	-0.656	0.900±0.412
HEB210409894	HXMT/CsI, GECAM	13.248±2.503	1.496	38.336±4.162	-0.936	13.022±4.535
HEB210411147	HXMT/CsI, Fermi-GBM (n8, n7)	36.672±0.345	-36.736	52.480±6.503	-44.160	4.507±1.120
HEB210421454	HXMT/CsI, Fermi-GBM (n3, n6, b0)	6.336±1.843	-3.816	29.568±5.257	-22.184	8.820±0.292
HEB210422572	HXMT/CsI, Fermi-GBM (n0, n1, b0)	6.528±1.180	3.040	38.464±6.728	-14.944	32.053±4.789
HEB210427206	HXMT/CsI, Fermi-GBM (n8, nb, b1)	8.064±0.264	1.752	32.000±3.019	-5.032	10.067±2.838
HEB210511476	HXMT/CsI, Fermi-GBM (n3, n5, b0)	1.792±0.091	3.176	5.824±0.580	1.064	5.008±0.708
HEB210515546	HXMT/CsI, Fermi-GBM (n9, na, b1)	0.960±0.286	-0.984	5.632±4.800	-1.176	10.017±4.480
HEB210516982	HXMT/CsI, Fermi-GBM (n2, na, b0)	2.816±0.453	5.308	7.872±0.389	4.924	7.012±2.065
HEB210518544	HXMT/CsI, Fermi-GBM (n8, nb, b1)	3.968±0.143	1.384	9.856±0.604	-2.264	12.521±5.394
HEB210520796	HXMT/CsI, Fermi-GBM (n0, n3, b0)	34.752±3.223	3.752	67.200±15.169	0.616	67.522±36.412
HEB210605214	HXMT/CsI, Fermi-GBM (n7, n8, b1)	0.192±0.091	-0.008	1.984±1.218	-0.072	0.200±0.014
HEB210606945	HXMT/CsI, Fermi-GBM (n3, n5, b0)	199.616±2.561	8.888	246.848±1.601	3.896	22.537±3.046
HEB210610827	HXMT/CsI, Fermi-GBM (n6, nb, b1)	17.344±0.202	5.264	67.392±3.917	-6.512	33.556±3.541
HEB210615981	HXMT/CsI, Fermi-GBM (n0, n3, b0)	0.832±0.143	-1.040	4.864±2.497	-3.920	5.008±1.120
HEB210622064	HXMT/CsI, Fermi-GBM (na, n8, b1)	27.456±5.588	1.072	48.256±5.824	-0.208	48.078±5.033
HEB210627311	HXMT/CsI, Fermi-GBM (n4, n5)	3.776±0.326	-0.216	9.024±0.516	-3.352	8.303±2.609

Table 5. Durations (40-800 keV for NG mode, 200-3000 keV for LG mode) of ‘SILVER’ and ‘BRONZE’ GRB samples

Trigger	Detectors	T_{50}	T_{50} start	T_{90}	T_{90} start
ID	Used	(s)	(s)	(s)	(s)
HEB170626040	HXMT/CsI	2.504±0.707	3.840	6.511±1.120	1.836
HEB170708045	HXMT/CsI	0.050±0.014	-0.004	0.200±0.022	-0.034
HEB170712139	HXMT/CsI	3.504±0.708	-2.628	8.511±1.119	-5.631
HEB170801208	HXMT/CsI	0.020±0.014	0.009	0.460±0.750	-0.421
HEB170803917	HXMT/CsI	0.160±0.014	0.837	0.260±0.014	0.787
HEB170805596	HXMT/CsI	0.040±0.032	0.192	0.270±0.487	-0.028
HEB170805610	HXMT/CsI	0.300±0.141	0.476	2.000±0.141	-1.024
HEB170829270	HXMT/CsI	2.002±0.707	0.374	5.507±2.696	-0.627
HEB170901499	HXMT/CsI	8.020±2.832	3.274	46.118±28.143	-0.736
HEB170904406	HXMT/CsI	5.901±0.224	2.475	11.403±0.608	0.175
HEB170904884	HXMT/CsI	2.002±0.707	10.888	10.012±3.645	7.384
HEB170918905	HXMT/CsI	0.540±0.033	0.312	1.929±0.310	0.162
HEB170921030	HXMT/CsI	0.500±0.071	-0.012	1.150±0.112	-0.312
HEB170926340	HXMT/CsI	89.223±5.111	0.750	108.270±18.073	-0.252
HEB171102106	HXMT/CsI	25.532±3.540	8.387	50.563±10.025	1.379
HEB171108279	HXMT/CsI	1.000±0.707	1.154	2.501±0.707	0.154
HEB171115217	HXMT/CsI	22.532±16.030	0.891	47.066±9.027	-14.130
HEB180103047	HXMT/CsI	43.310±33.511	-7.728	55.813±3.516	-16.630
HEB180103949	HXMT/CsI	0.160±0.014	0.928	0.430±0.149	0.888
HEB180112687	HXMT/CsI	138.168±1.119	1.380	158.193±26.537	-4.127
HEB180202211	HXMT/CsI	2.503±0.708	2.378	8.511±1.119	-0.125
HEB180210728	HXMT/CsI	4.005±2.064	0.876	14.018±4.036	-0.125
HEB180221520	HXMT/CsI	11.503±2.802	7.277	32.208±6.902	1.776
HEB180226392	HXMT/CsI	0.200±0.141	0.476	1.400±0.412	0.376
HEB180326143	HXMT/CsI	7.017±2.242	3.759	14.035±1.414	2.757
HEB180405168	HXMT/CsI	9.011±2.064	6.382	22.528±3.540	0.875
HEB180411359	HXMT/CsI	47.559±2.239	39.928	94.617±5.529	6.386
HEB180603235	HXMT/CsI	0.200±0.071	0.088	0.450±0.461	-0.012
HEB180617871	HXMT/CsI	0.200±0.141	-0.131	1.200±0.141	-1.031
HEB180626260	HXMT/CsI	19.048±1.416	0.751	25.063±8.267	-2.256
HEB180704525	HXMT/CsI	5.012±1.416	1.752	13.032±4.133	-1.256
HEB180804554	HXMT/CsI	10.025±1.416	0.751	27.067±3.169	-9.273
HEB181011181	HXMT/CsI	4.010±1.416	1.753	8.020±1.416	0.750
HEB181201111	HXMT/CsI	5.401±0.141	4.177	20.605±1.118	-1.324
HEB190102652	HXMT/CsI	1.898±0.122	4.059	2.918±0.349	3.449
HEB190117608	HXMT/CsI	15.704±0.412	2.176	21.805±1.504	0.375
HEB190203655	HXMT/CsI	25.062±2.241	-22.307	60.149±14.071	-42.357

Table 5 continued

Table 5 (*continued*)

Trigger	Detectors	T_{50}	T_{50} start	T_{90}	T_{90} start
ID	Used	(s)	(s)	(s)	(s)
HEB190212129	HXMT/CsI	0.045±0.090	-0.007	0.180±0.335	-0.027
HEB190218810	HXMT/CsI	16.704±6.802	6.177	29.807±7.803	0.175
HEB190306467	HXMT/CsI	19.048±2.241	0.751	29.073±7.635	-4.261
HEB190321931	HXMT/CsI	4.506±0.707	0.877	8.511±1.119	0.377
HEB190323878	HXMT/CsI	14.017±0.708	1.878	25.031±3.206	-3.629
HEB190330207	HXMT/CsI	0.520±0.360	-0.473	3.400±1.840	-1.453
HEB190331841	HXMT/CsI	0.050±0.071	0.039	0.850±0.255	-0.761
HEB190510119	HXMT/CsI	47.117±9.078	11.780	76.190±11.073	0.752
HEB190605110	HXMT/CsI	6.402±0.707	2.676	15.704±2.702	0.275
HEB190610477	HXMT/CsI	0.200±0.141	1.075	0.500±0.141	0.975
HEB190615612	HXMT/CsI	20.050±1.416	1.753	29.072±4.133	0.751
HEB190706710	HXMT/CsI	1.502±0.708	-0.125	2.503±0.707	-0.125
HEB190719113	HXMT/CsI	6.007±3.645	-6.131	10.513±2.239	-7.132
HEB190825878	HXMT/CsI	14.035±1.416	2.757	28.070±5.111	-0.251
HEB190828783	HXMT/CsI	3.004±0.707	0.375	5.006±0.708	-0.125
HEB190831271	HXMT/CsI	0.400±0.141	1.077	2.601±0.141	-1.024
HEB190906045	HXMT/CsI	0.030±0.014	0.019	0.060±0.014	-0.001
HEB190927106	HXMT/CsI	20.050±2.241	5.765	34.085±6.340	1.755
HEB190928550	HXMT/CsI	5.012±1.416	97.993	27.067±2.242	81.953
HEB190928551	HXMT/CsI	5.006±0.707	3.881	21.026±0.708	-7.133
HEB190929884	HXMT/CsI	16.040±1.418	-2.256	43.108±3.170	-23.309
HEB191021831	HXMT/CsI	2.503±0.708	0.375	9.011±0.708	-5.131
HEB191031182	HXMT/CsI	3.101±0.316	1.876	9.502±0.447	0.275
HEB191031318	HXMT/CsI	3.007±1.418	4.761	9.022±1.416	0.751
HEB191119445	HXMT/CsI	0.040±0.007	0.019	0.095±0.007	0.004
HEB191202378	HXMT/CsI	3.008±1.414	-3.259	3.008±1.414	-3.259
HEB191224829	HXMT/CsI	1.700±0.224	0.476	2.901±0.922	-0.524
HEB200211193	HXMT/CsI	0.000±2.242	-0.249	3.007±1.416	-2.254
HEB200313878	HXMT/CsI	1.850±0.212	0.238	3.300±0.552	-0.112
HEB200326421	HXMT/CsI	77.628±9.070	9.350	97.160±16.034	1.838
HEB200413712	HXMT/CsI	0.900±0.224	0.075	2.201±0.316	-0.125
HEB200413743	HXMT/CsI	2.501±0.825	-0.124	8.702±0.721	-2.224
HEB200521511	HXMT/CsI	0.150±0.014	-0.587	0.590±0.041	-0.647
HEB200526628	HXMT/CsI	7.017±1.418	62.907	73.182±12.072	3.759
HEB201122355	HXMT/CsI	6.511±0.708	1.338	9.516±2.554	0.837
HEB210124558	HXMT/CsI	0.020±0.014	3.069	0.500±0.114	2.769
HEB210129908	HXMT/CsI	2.401±0.224	0.667	18.606±4.806	-0.433
HEB210208564	HXMT/CsI	24.216±1.020	0.738	25.216±1.078	0.337
HEB210213286	HXMT/CsI	10.934±1.729	3.182	18.886±2.225	1.194
HEB210306320	HXMT/CsI	8.027±2.242	5.685	29.097±1.417	1.671

Table 5 continued

Table 5 (*continued*)

Trigger	Detectors	T_{50}	T_{50} start	T_{90}	T_{90} start
ID	Used	(s)	(s)	(s)	(s)
HEB210306879	HXMT/CsI	3.010 ± 1.414	1.673	8.027 ± 1.417	-0.334
HEB210326890	HXMT/CsI	11.037 ± 2.838	-4.349	13.043 ± 3.173	-5.353
HEB210328396	HXMT/CsI	3.101 ± 2.885	-1.934	5.002 ± 0.671	-2.235
HEB210405507	HXMT/CsI	2.000 ± 0.071	-1.267	7.051 ± 1.801	-3.017
HEB210406716	HXMT/CsI	8.504 ± 1.119	3.776	17.008 ± 3.537	0.774
HEB210429071	HXMT/CsI	10.517 ± 1.584	1.840	34.056 ± 9.529	-9.679
HEB210502295	HXMT/CsI	2.003 ± 1.120	1.838	8.013 ± 0.708	1.337
HEB210504958	HXMT/CsI	14.023 ± 7.529	2.337	54.090 ± 14.104	-9.182
HEB210506027	HXMT/CsI	0.400 ± 0.453	-0.415	1.200 ± 0.255	-1.215
HEB210511647	HXMT/CsI	10.033 ± 6.103	6.688	45.150 ± 9.085	0.668
HEB210602502	HXMT/CsI	0.501 ± 0.707	1.335	2.003 ± 0.707	0.834
HEB210606120	HXMT/CsI	2.200 ± 0.071	1.784	4.951 ± 0.255	0.834
HEB210607775	HXMT/CsI	9.030 ± 3.172	0.667	15.050 ± 5.676	-0.336
HEB210607902	HXMT/CsI	7.202 ± 0.224	0.370	16.705 ± 2.603	-2.831
HEB210615891	HXMT/CsI	13.043 ± 6.103	-0.335	24.080 ± 6.731	-1.338
HEB210622339	HXMT/CsI	2.001 ± 0.224	3.068	6.402 ± 1.265	0.367
HEB210627813	HXMT/CsI	79.264 ± 26.106	3.678	104.347 ± 11.218	-8.362

Table 6. Fluence and Peak Flux (10–2000 keV) from joint analyses with ‘GOLDEN’ GRB samples.

Trigger	Fluence	PF64	PF256	PF1024
ID	(erg cm $^{-2}$)	(ph cm $^{-2}$ s $^{-1}$)	(ph cm $^{-2}$ s $^{-1}$)	(ph cm $^{-2}$ s $^{-1}$)
HEB170626400	1.54e-05±1.43e-07	41.78±3.65	38.89±1.64	32.66±0.68
HEB170705115	2.03e-05±6.04e-07	40.64±7.53	32.12±3.08	21.31±1.22
HEB170714049	2.31e-07±2.72e-08	6.08±1.26	2.52±0.38	0.85±0.11
HEB170718152	2.29e-06±5.94e-08	3.50±0.75	2.21±0.31	1.57±0.12
HEB170726248	1.50e-06±1.01e-07	4.55±0.92	3.07±0.43	2.19±0.18
HEB170726793	8.23e-06±1.08e-07	11.03±1.07	7.71±0.43	3.79±0.16
HEB170728960	4.36e-06±9.99e-08	24.14±2.25	21.56±1.09	11.19±0.38
HEB170731751	3.07e-06±9.91e-07	1.89±0.51	1.10±0.21	0.75±0.08
HEB170802637	3.13e-06±1.78e-07	36.30±3.41	26.20±1.38	8.57±0.39
HEB170817908	5.50e-06±9.30e-08	14.55±0.86	10.09±0.42	6.79±0.17
HEB170825306	7.82e-06±1.68e-07	9.55±1.40	7.81±0.62	6.60±0.29
HEB170826818	3.90e-05±3.48e-07	47.94±3.55	40.70±1.58	28.39±0.65
HEB170903534	5.70e-06±9.44e-08	4.55±0.31	3.25±0.15	2.72±0.07
HEB170906029	1.46e-04±7.09e-07	32.61±3.52	30.36±1.50	24.44±0.66
HEB170912984	1.68e-06±2.14e-07	4.44±0.78	2.12±0.30	0.65±0.09
HEB170923188	4.86e-06±1.20e-07	7.19±0.38	4.95±0.16	3.68±0.08
HEB171008079	1.60e-06±9.14e-08	4.53±0.71	3.85±0.33	1.59±0.11
HEB171013350	2.19e-05±2.65e-07	11.40±2.10	8.70±0.91	7.67±0.43
HEB171020963	3.75e-06±1.39e-07	21.76±2.22	10.98±0.84	4.78±0.32
HEB171030728	1.92e-07±2.22e-08	8.26±1.05	4.17±0.38	1.08±0.09
HEB171103965	2.82e-06±8.49e-08	14.01±0.83	10.49±0.41	3.16±0.11
HEB171120555	2.95e-05±3.04e-07	87.57±6.19	78.60±2.98	45.05±1.02
HEB171124234	2.06e-05±4.72e-07	4.21±0.60	3.30±0.25	2.39±0.10
HEB171207054	6.60e-07±5.57e-08	5.78±0.53	4.00±0.27	1.25±0.08
HEB171209615	9.77e-06±2.53e-07	5.03±0.56	3.34±0.23	1.73±0.16
HEB171210492	1.24e-04±6.12e-07	15.06±1.96	13.21±0.81	12.68±0.37
HEB171215705	7.76e-06±1.35e-07	3.55±0.64	2.50±0.23	2.11±0.11
HEB171223818	1.33e-08±7.50e-09	1.26±0.46	0.76±0.20	0.09±0.07
HEB171230955	2.39e-05±2.82e-07	8.74±1.50	6.85±0.77	5.85±0.34
HEB180110608	2.01e-06±1.16e-07	3.57±0.81	2.83±0.37	1.70±0.14
HEB180111695	6.22e-05±1.10e-06	56.11±9.30	42.25±3.60	33.46±1.63
HEB180119836	2.86e-06±8.67e-08	6.98±0.58	5.77±0.25	4.56±0.11
HEB180127049	5.47e-06±1.60e-07	4.19±0.41	2.79±0.29	2.36±0.16
HEB180130744	1.62e-07±2.19e-08	4.36±0.55	2.54±0.22	0.75±0.06
HEB180208764	4.91e-06±3.92e-07	4.06±0.58	2.95±0.82	2.26±0.33
HEB180210517	5.60e-05±4.09e-07	28.01±3.27	24.69±1.41	18.70±0.66
HEB180305393	8.20e-05±8.81e-07	44.44±4.73	42.08±2.29	36.97±1.07

Table 6 continued

Table 6 (*continued*)

Trigger	Fluence	PF64	PF256	PF1024
ID	(erg cm ⁻²)	(ph cm ⁻² s ⁻¹)	(ph cm ⁻² s ⁻¹)	(ph cm ⁻² s ⁻¹)
HEB180306972	2.85e-06±8.88e-08	1.87±0.40	1.18±0.15	0.78±0.06
HEB180309321	9.51e-06±1.64e-07	5.73±1.66	4.24±0.60	3.43±0.27
HEB180313977	6.39e-07±1.10e-07	14.12±2.27	4.34±0.66	1.20±0.18
HEB180330891	8.47e-06±1.93e-07	11.90±1.31	10.72±0.54	9.88±0.26
HEB180331177	2.08e-06±7.76e-08	1.51±0.27	0.76±0.10	0.33±0.04
HEB180401279	8.81e-06±2.53e-07	7.06±1.31	6.50±0.81	4.07±0.32
HEB180402406	8.02e-07±5.41e-08	7.83±0.98	4.43±0.33	1.22±0.08
HEB180404091	2.11e-05±1.47e-07	5.83±0.64	4.99±0.31	4.24±0.14
HEB180409346	3.32e-05±4.14e-07	118.01±11.41	91.04±4.74	56.26±1.78
HEB180413117	7.18e-06±1.97e-06	4.29±0.92	3.34±0.44	2.70±0.19
HEB180416923	3.45e-05±4.21e-07	9.31±1.22	8.26±0.57	5.88±0.26
HEB180427442	5.67e-05±6.24e-07	41.34±6.21	38.76±3.33	35.75±1.50
HEB180505539	2.68e-05±1.76e-07	53.94±1.88	49.43±1.14	37.11±0.49
HEB180506902	3.38e-06±6.13e-08	4.08±0.68	2.85±0.29	2.52±0.13
HEB180510808	7.00e-06±4.98e-07	19.59±3.94	18.01±2.18	12.69±0.81
HEB180523782	1.57e-06±5.40e-08	7.06±0.80	4.52±0.33	2.55±0.13
HEB180525151	4.32e-07±3.67e-08	8.90±1.18	4.10±0.39	1.18±0.10
HEB180605457	2.37e-05±2.79e-07	16.99±1.36	12.39±0.66	6.48±0.25
HEB180618030	3.23e-06±9.93e-08	15.00±0.83	12.74±0.33	4.52±0.15
HEB180623696	2.28e-05±5.31e-07	10.11±1.79	7.95±0.96	6.53±0.43
HEB180625940	1.36e-06±1.66e-07	5.32±2.01	4.31±0.79	1.95±0.25
HEB180626391	6.60e-07±4.14e-08	16.39±1.84	4.88±0.50	2.67±0.19
HEB180704233	1.28e-05±1.88e-07	5.25±0.78	4.14±0.36	3.30±0.16
HEB180715754	1.49e-06±7.43e-08	5.00±0.86	4.07±0.39	2.18±0.13
HEB180718762	2.73e-05±1.82e-06	5.34±1.00	4.31±0.54	3.71±0.25
HEB180722992	2.93e-05±1.84e-07	10.41±1.43	8.89±0.61	8.26±0.30
HEB180724807	5.73e-05±4.46e-07	16.05±1.84	13.90±0.87	12.89±0.45
HEB180730017	2.32e-07±9.46e-08	11.60±1.08	5.39±0.54	1.19±0.19
HEB180801275	9.74e-07±6.16e-08	6.67±0.80	4.36±0.34	1.85±0.11
HEB180803590	1.82e-07±1.93e-08	3.25±0.57	2.02±0.23	0.61±0.06
HEB180804930	7.25e-06±1.19e-07	10.53±1.21	9.99±0.61	7.34±0.24
HEB180816088	2.21e-05±2.07e-07	21.94±2.73	18.92±1.30	15.40±0.57
HEB180822561	3.65e-06±9.97e-08	4.75±0.96	3.98±0.42	3.30±0.18
HEB180828789	3.41e-05±3.65e-07	48.57±4.57	39.89±1.88	34.42±0.84
HEB180925407	7.12e-07±3.94e-08	3.10±0.46	1.91±0.17	0.75±0.06
HEB180925609	1.42e-05±2.73e-07	27.34±3.14	23.90±1.48	12.13±0.55
HEB180927992	2.54e-06±9.05e-08	7.12±0.95	5.84±0.38	4.41±0.18
HEB180929453	1.57e-06±6.08e-08	6.47±0.90	5.47±0.38	3.14±0.15
HEB181008269	1.63e-05±1.30e-07	15.12±1.65	13.21±0.86	12.62±0.40
HEB181014479	1.65e-05±1.56e-07	6.50±0.68	5.66±0.36	5.05±0.18

Table 6 continued

Table 6 (*continued*)

Trigger	Fluence	PF64	PF256	PF1024
ID	(erg cm ⁻²)	(ph cm ⁻² s ⁻¹)	(ph cm ⁻² s ⁻¹)	(ph cm ⁻² s ⁻¹)
HEB181028590	2.76e-05±1.98e-07	13.74±1.11	11.80±0.59	9.63±0.27
HEB181119605	2.05e-05±2.16e-07	39.74±3.90	33.25±1.96	21.97±0.67
HEB181121306	6.90e-07±1.17e-07	3.83±1.15	3.02±0.67	1.10±0.19
HEB181122381	8.18e-06±2.08e-07	10.88±1.59	8.80±0.68	4.15±0.21
HEB181123231	6.71e-07±4.43e-08	6.41±0.32	5.00±0.40	1.64±0.11
HEB181212692	2.24e-05±1.82e-07	61.54±3.12	59.15±1.56	52.87±0.81
HEB181213540	7.43e-06±2.70e-07	7.95±1.62	3.43±0.53	2.24±0.21
HEB181217664	1.31e-05±2.38e-07	18.60±2.40	7.81±0.73	6.69±0.35
HEB181225489	1.12e-05±3.06e-07	10.46±1.55	8.99±0.70	7.62±0.29
HEB190103877	2.46e-05±3.88e-07	2.77±0.33	2.51±0.19	2.25±0.09
HEB190110725	4.38e-06±7.96e-08	13.22±1.22	12.17±0.66	9.64±0.32
HEB190131964	8.52e-06±1.14e-07	1.72±0.23	1.28±0.11	1.05±0.05
HEB190215771	1.59e-05±1.30e-07	8.95±0.82	8.53±0.53	8.09±0.24
HEB190222537	2.96e-05±7.61e-07	23.19±4.54	18.91±2.11	16.31±1.00
HEB190226515	1.26e-06±1.09e-07	11.37±1.73	8.92±0.72	2.43±0.19
HEB190310398	2.41e-05±2.51e-07	28.43±2.97	26.74±1.43	25.69±0.79
HEB190324348	2.44e-05±1.78e-07	8.43±0.81	7.53±0.43	6.96±0.20
HEB190324947	1.86e-05±2.39e-07	28.98±3.78	26.53±1.57	22.22±0.65
HEB190326313	1.39e-05±1.35e-07	11.25±1.03	9.30±0.50	7.24±0.23
HEB190326316	1.32e-07±1.57e-08	2.21±0.36	0.70±0.10	0.22±0.03
HEB190330694	1.09e-05±1.63e-07	8.19±1.24	7.42±0.50	6.80±0.24
HEB190331093	3.17e-06±1.07e-07	2.15±0.49	1.76±0.23	1.01±0.08
HEB190401139	1.94e-05±1.73e-07	19.20±1.93	16.36±1.13	14.34±0.51
HEB190407671	1.13e-05±2.70e-07	23.27±3.59	13.65±1.32	11.23±0.57
HEB190422283	3.09e-05±1.94e-07	16.17±1.77	15.35±0.86	12.94±0.39
HEB190424417	1.17e-05±4.28e-07	22.26±3.40	10.24±1.46	6.58±0.59
HEB190507269	3.31e-06±6.19e-08	5.10±0.87	3.94±0.38	3.16±0.16
HEB190515189	8.68e-07±5.45e-08	4.59±0.56	4.18±0.35	1.56±0.10
HEB190525031	1.93e-06±8.58e-08	7.06±0.94	5.41±0.40	3.03±0.14
HEB190531840	1.08e-04±4.73e-07	51.13±2.41	45.02±1.14	39.16±0.59
HEB190604446	2.26e-05±2.77e-07	18.51±2.13	17.25±0.97	13.67±0.46
HEB190613449	5.45e-06±1.52e-07	3.01±0.39	2.21±0.17	1.74±0.07
HEB190615636	1.20e-05±3.67e-07	7.05±1.45	5.41±0.71	4.31±0.36
HEB190619594	4.04e-05±3.76e-07	20.59±3.09	16.21±1.14	14.13±0.55
HEB190620507	5.95e-05±2.93e-07	18.17±1.30	16.91±0.69	16.09±0.35
HEB190720964	3.51e-06±7.89e-08	5.61±0.84	4.82±0.42	4.52±0.19
HEB190723308	3.29e-06±9.60e-08	4.10±0.75	3.46±0.35	2.61±0.16
HEB190724030	3.94e-07±2.15e-08	9.93±0.62	3.26±0.19	0.84±0.05
HEB190726642	1.73e-05±2.36e-07	21.73±3.33	20.74±1.49	19.26±0.67
HEB190806675	8.17e-06±1.16e-07	4.31±0.68	3.30±0.24	2.54±0.11

Table 6 continued

Table 6 (*continued*)

Trigger	Fluence	PF64	PF256	PF1024
ID	(erg cm ⁻²)	(ph cm ⁻² s ⁻¹)	(ph cm ⁻² s ⁻¹)	(ph cm ⁻² s ⁻¹)
HEB190813520	3.99e-07±6.00e-08	9.41±2.10	3.58±0.60	1.03±0.16
HEB190814837	1.85e-06±5.81e-08	1.62±0.32	1.16±0.13	0.97±0.06
HEB190901890	4.38e-05±3.68e-07	19.34±1.86	16.48±0.93	15.77±0.45
HEB190903721	4.43e-07±2.49e-08	2.99±0.35	1.82±0.13	0.67±0.04
HEB190906767	4.91e-06±3.40e-07	10.55±1.01	8.50±0.43	5.48±0.20
HEB190915239	7.11e-06±2.21e-07	6.74±1.77	5.29±0.67	4.46±0.31
HEB191009297	1.90e-05±5.31e-07	2.84±0.74	2.05±0.31	1.72±0.15
HEB191019970	3.80e-05±2.53e-07	7.56±1.02	6.71±0.50	6.15±0.23
HEB191031780	1.14e-05±1.34e-07	6.46±1.03	4.64±0.40	3.78±0.18
HEB191105257	6.39e-06±6.99e-08	60.97±0.94	45.59±0.38	11.92±0.12
HEB191108003	2.28e-05±3.92e-07	7.96±2.45	5.64±0.93	3.85±0.40
HEB191111364	2.29e-05±2.60e-07	28.32±4.07	17.58±1.57	12.28±0.64
HEB191113578	1.06e-06±6.93e-08	10.79±1.97	6.66±0.78	4.94±0.33
HEB191118925	6.14e-06±1.09e-07	4.39±0.79	3.28±0.31	2.94±0.15
HEB191130506	9.57e-06±1.51e-07	3.47±0.56	2.34±0.22	1.91±0.10
HEB191202867	2.86e-05±3.29e-07	42.80±4.69	38.55±2.02	28.30±0.89
HEB191203289	3.68e-07±4.30e-08	2.62±0.74	1.99±0.33	0.88±0.10
HEB191205740	9.49e-07±6.24e-08	4.73±0.79	3.31±0.34	1.59±0.13
HEB191218112	2.70e-05±2.27e-07	7.06±0.92	6.30±0.41	5.81±0.20
HEB191221860	6.98e-05±6.41e-07	48.23±4.60	45.41±2.25	35.96±0.95
HEB191227069	6.11e-05±2.67e-07	42.03±1.88	37.79±0.99	31.34±0.46
HEB200109073	5.49e-06±2.20e-07	2.50±1.04	1.46±0.36	1.09±0.14
HEB200111632	6.22e-06±1.71e-07	20.45±2.09	17.01±0.96	10.95±0.39
HEB200114153	6.83e-06±1.43e-07	2.43±0.63	2.19±0.28	1.84±0.12
HEB200120961	1.24e-05±2.82e-07	38.90±6.14	25.40±1.85	18.08±0.83
HEB200125863	5.92e-05±4.54e-07	175.35±9.57	149.25±3.78	110.27±1.63
HEB200219998	3.21e-05±3.67e-07	32.78±2.79	29.51±1.56	25.39±0.73
HEB200221161	2.50e-06±2.37e-07	6.13±2.10	5.09±0.93	2.78±0.30
HEB200227305	1.26e-05±1.20e-07	10.07±1.10	7.57±0.53	6.81±0.24
HEB200323782	4.06e-06±1.07e-07	37.44±3.94	33.41±1.97	26.08±0.91
HEB200325137	2.92e-06±1.06e-07	9.81±1.00	7.43±0.43	4.91±0.17
HEB200326517	7.86e-07±3.70e-08	0.98±0.16	0.77±0.08	0.46±0.03
HEB200412381	8.70e-05±5.97e-07	157.21±8.23	155.41±3.77	115.72±1.58
HEB200416295	1.36e-06±4.05e-08	5.44±0.48	4.37±0.22	3.28±0.09
HEB200418864	1.85e-06±1.10e-07	5.33±1.44	3.39±0.59	2.02±0.23
HEB200519472	1.06e-05±3.27e-07	9.88±1.77	8.16±0.90	7.09±0.41
HEB200601097	5.41e-05±5.02e-07	7.88±1.82	5.44±0.72	4.80±0.31
HEB200609379	3.13e-05±2.80e-07	4.49±0.76	4.07±0.32	3.28±0.14
HEB200617679	1.81e-06±2.20e-07	5.09±1.10	4.06±0.50	1.98±0.20
HEB200619108	9.97e-06±1.30e-07	4.48±0.43	4.09±0.23	3.62±0.11

Table 6 continued

Table 6 (*continued*)

Trigger	Fluence	PF64	PF256	PF1024
ID	(erg cm ⁻²)	(ph cm ⁻² s ⁻¹)	(ph cm ⁻² s ⁻¹)	(ph cm ⁻² s ⁻¹)
HEB200707072	4.18e-06±1.11e-07	2.47±0.58	1.88±0.22	1.27±0.09
HEB200711461	3.00e-05±4.65e-07	28.38±3.22	25.64±1.56	19.43±0.68
HEB200716315	4.07e-05±4.25e-07	11.31±1.48	9.04±0.58	7.90±0.27
HEB200716956	2.00e-05±3.78e-07	34.45±1.42	23.98±0.63	7.99±0.18
HEB200801352	4.38e-06±8.90e-08	1.30±0.28	0.83±0.10	0.61±0.04
HEB200806645	1.37e-05±1.99e-07	11.20±1.50	9.68±0.62	6.39±0.25
HEB200809653	3.77e-06±8.93e-08	8.01±0.74	5.73±0.31	4.24±0.14
HEB200824594	3.06e-07±3.02e-08	1.62±0.28	1.29±0.15	0.77±0.06
HEB200903112	1.15e-05±2.16e-07	2.15±0.62	1.78±0.30	1.40±0.13
HEB200919964	8.60e-05±6.26e-07	24.42±2.36	17.77±0.98	14.62±0.52
HEB200922504	2.58e-06±9.06e-08	2.58±0.50	1.91±0.20	1.56±0.10
HEB200928551	7.23e-06±9.80e-08	8.70±0.92	6.24±0.37	4.09±0.18
HEB201013157	1.56e-05±1.72e-07	41.55±2.06	40.47±1.05	33.90±0.54
HEB201105229	3.91e-05±2.84e-07	28.91±2.38	27.41±1.08	25.41±0.51
HEB201209239	1.60e-05±5.13e-07	4.86±1.15	3.29±0.43	2.71±0.19
HEB201221591	5.96e-07±4.37e-08	45.36±2.95	12.27±0.93	3.77±0.32
HEB201226553	8.34e-06±1.24e-07	2.19±0.43	1.81±0.19	1.31±0.08
HEB210112068	5.71e-05±1.06e-06	85.78±11.81	67.83±5.27	40.40±2.00
HEB210119120	2.37e-07±3.17e-08	10.73±1.43	2.85±0.38	0.71±0.10
HEB210121779	1.19e-04±5.64e-07	32.48±2.08	27.75±0.82	25.45±0.39
HEB210123304	2.22e-05±2.21e-07	37.27±3.04	29.43±1.36	25.53±0.68
HEB210207911	1.05e-04±1.66e-06	120.06±14.20	102.50±7.03	74.98±2.84
HEB210225217	6.73e-06±1.04e-07	4.32±0.80	3.72±0.31	3.19±0.15
HEB210227114	1.46e-05±3.48e-07	2.09±0.45	1.94±0.20	1.40±0.09
HEB210228057	4.76e-06±1.30e-07	9.87±1.08	7.77±0.51	6.03±0.22
HEB210307247	8.97e-07±7.74e-08	5.94±1.31	3.40±0.52	1.36±0.15
HEB210323918	2.08e-06±4.48e-08	33.52±0.93	20.39±0.38	6.39±0.14
HEB210324468	1.28e-05±1.08e-07	10.31±0.61	4.78±0.22	3.82±0.11
HEB210326057	4.51e-07±4.08e-08	4.45±0.92	2.79±0.30	0.87±0.08
HEB210409894	8.86e-06±1.72e-07	2.99±0.71	2.47±0.36	2.22±0.16
HEB210411147	7.29e-06±1.47e-07	2.69±0.48	2.47±0.19	1.83±0.09
HEB210421454	4.75e-06±1.83e-07	2.84±0.85	2.57±0.33	2.15±0.17
HEB210422572	4.65e-06±1.17e-07	1.46±0.32	1.19±0.12	0.98±0.06
HEB210427206	2.09e-05±4.31e-07	17.65±1.38	13.88±0.61	10.90±0.27
HEB210511476	1.18e-05±1.96e-07	37.13±4.20	34.30±2.04	30.68±0.96
HEB210515546	5.28e-07±3.58e-08	1.30±0.24	0.96±0.12	0.66±0.05
HEB210516982	2.90e-06±7.91e-08	10.00±0.84	8.76±0.36	6.31±0.16
HEB210518544	9.26e-06±2.14e-07	24.45±4.85	18.60±1.71	16.11±0.85
HEB210520796	7.88e-06±1.53e-07	2.02±0.39	1.68±0.16	1.24±0.07
HEB210605214	2.17e-06±4.92e-08	17.98±0.57	14.47±0.26	5.10±0.10

Table 6 continued

Table 6 (*continued*)

Trigger	Fluence	PF64	PF256	PF1024
ID	(erg cm ⁻²)	(ph cm ⁻² s ⁻¹)	(ph cm ⁻² s ⁻¹)	(ph cm ⁻² s ⁻¹)
HEB210606945	5.53e-05±5.01e-07	63.48±1.48	48.28±0.62	37.22±0.27
HEB210610827	6.59e-05±3.26e-07	22.63±1.77	21.94±0.84	19.24±0.41
HEB210615981	9.91e-07±5.46e-08	2.20±0.44	1.55±0.19	1.21±0.08
HEB210622064	5.65e-06±1.42e-07	3.68±0.50	2.94±0.23	2.06±0.10
HEB210627311	1.28e-06±7.19e-08	4.11±1.32	2.83±0.44	2.27±0.20

APPENDIX

A. LIGHT CURVES AND SPECTRA OF GRB 200125B AND GRB 210121A

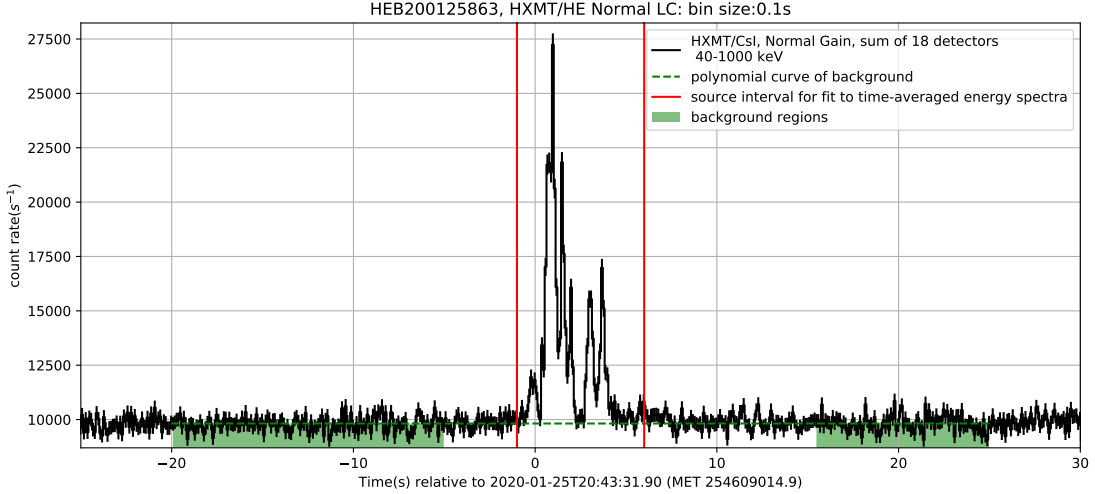


Figure 17. Light curve of GRB 200125B (HEB200125863) of 18 CsI detectors. Vertical lines indicate the regions selected for the fit to the time-averaged spectra. Green regions defines the background region. Here MET means the mission elapsed time of HXMT.

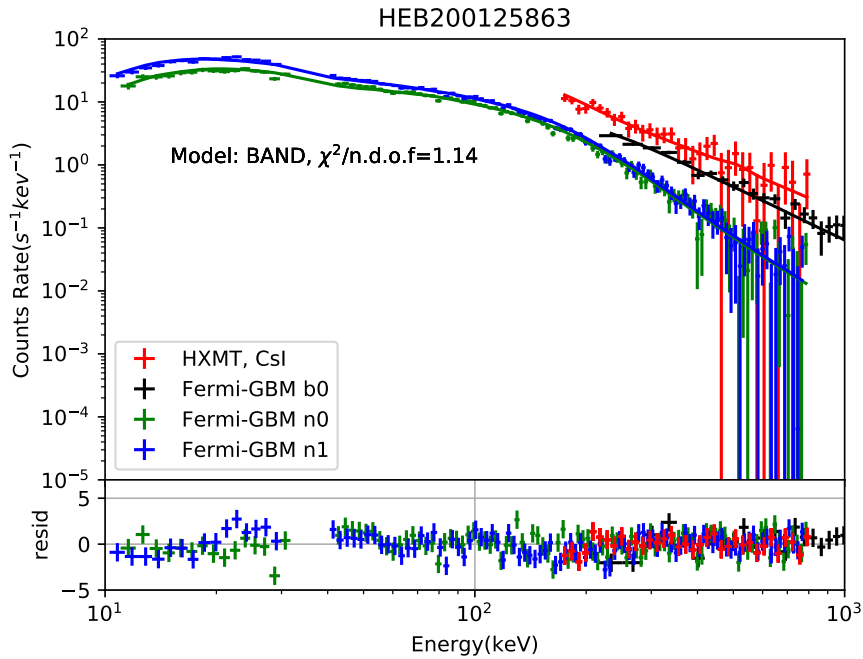


Figure 18. Joint analysis of time-averaged spectrum of GRB 200125B (HEB200125863). Data from 18 HXMT/CsI detectors and *Fermi*/GBM NaI detector 0, 1, BGO detector 0 are utilized.

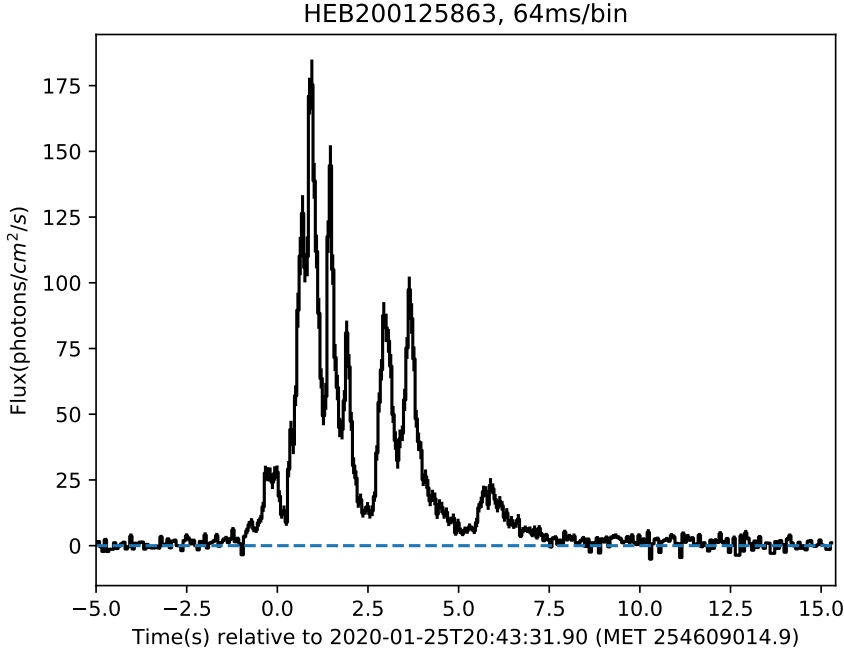


Figure 19. Photon flux light curve for GRB 200125B (HEB200125863) produced by the duration analysis. Data from 18 HE/CsI detectors and *Fermi*/GBM NaI detector 0, 1, BGO detector 0 are used. Here MET means the mission elapsed time of HXMT.

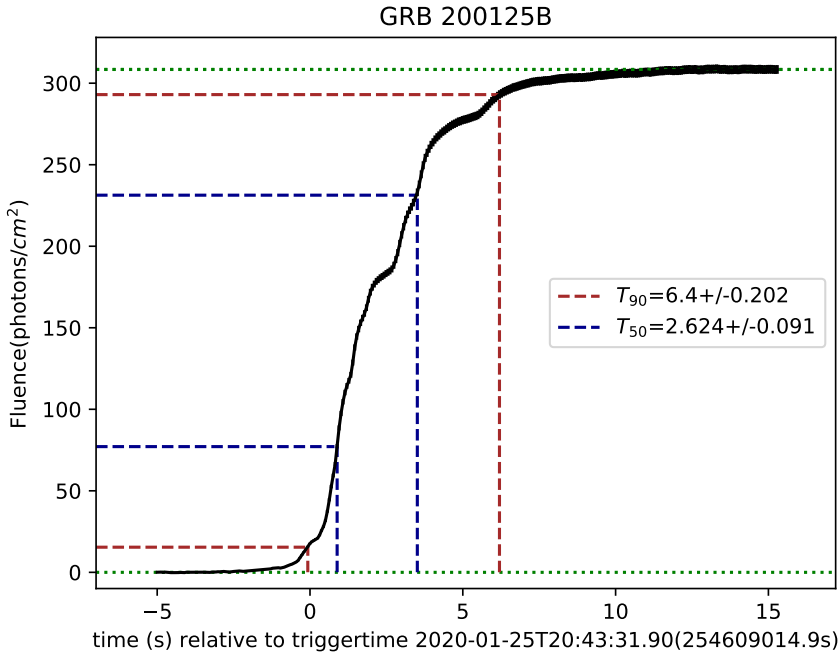


Figure 20. The duration plot for GRB 200125B (HEB200125863). Horizontal dashed lines in dark red are drawn at 5% and 95% of the total fluence, while those in dark blue at 25% and 75%. Vertical dotted lines are drawn at the times corresponding to those same fluences, thereby defining the T_{50} and T_{90} intervals. The green dotted horizontal lines are corresponding to the 0% and 100% of the total integration of the flux respectively. Here MET means the mission elapsed time of HXMT.

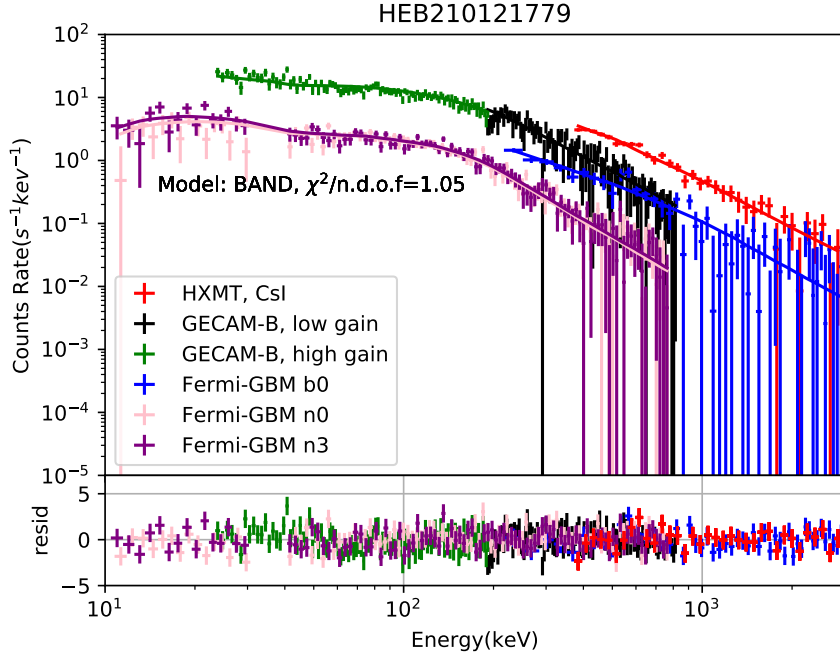


Figure 21. Joint analysis of time-averaged spectrum of GRB 210121A (HEB210121779). Data from 18 HE/CsI detectors and *Fermi*/GBM NaI detector 0, 3, BGO detector 0 are utilized.

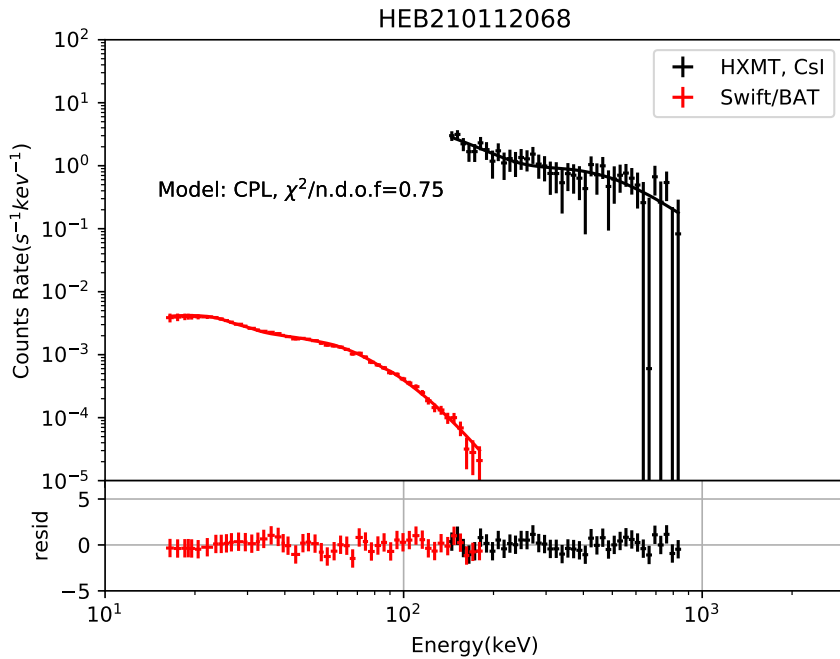


Figure 22. Joint analysis of time-averaged spectrum of GRB 210112A (HEB210112068). Data from 18 HE/CsI detectors and *Swift*/BAT are utilized.

REFERENCES

- Agostinelli, S., Allison, J., Amako, K., et al. 2003, Nuclear Instruments & Methods in Physics Research, 506, 250
- Band, D., Matteson, J., Ford, L., et al. 1993, ApJ, 413, 281
- Blackburn, L., Briggs, M. S., Camp, J., et al. 2015, ApJS, 217, 8. <https://doi.org/10.1088/0067-0049/217/1/8>
- Cai, C., Xiong, S. L., Li, C. K., et al. 2021, MNRAS, <https://academic.oup.com/mnras/advance-article-pdf/doi/10.1093/mnras/stab2760/40440234/stab2760.pdf>. <https://doi.org/10.1093/mnras/stab2760>
- Cao, X. L., Jiang, W. C., Meng, B., Zhang, W. C., & Luo, T. 2020, Sci. China-Phys. Mech. Astron., 63, arXiv:1910.04451
- Cash, W. 1979, ApJ, 228, 939
- Chen, Y., Cui, W. W., Li, W., et al. 2020, Sci. China-Phys. Mech. Astron. 63, 249505, 63, arXiv:1910.08319
- Goldstein, A., Burns, E., Hamburg, R., et al. 2016, arXiv e-prints, arXiv:1612.02395
- Goldstein, A., Burgess, J. M., Preece, R. D., et al. 2012, ApJS, 199, 19. <https://doi.org/10.1088/0067-0049/199/1/19>
- Goldstein, A., Hamburg, R., Wood, J., et al. 2019, arXiv e-prints, arXiv:1903.12597
- Guidorzi, C., Orlandini, M., Frontera, F., et al. 2020, A&A, 642, A160
- Hurley, K., Briggs, M. S., Kippen, R. M., et al. 1999, ApJS, 120, 399. <https://doi.org/10.1086/313178>
- Ishida, M., Tsujimoto, M., Kohmura, T., et al. 2014, Publications of the Astronomical Society of Japan, 63, S657
- Kocevski, D., Burns, E., Goldstein, A., et al. 2018, ApJ, 862, 152. <https://doi.org/10.3847/1538-4357/aacb7b>
- Koshut, T. M., Paciesas, W. S., Kouveliotou, C., et al. 1996, ApJ, 463, 570
- Li, T. P., Xiong, S. L., Zhang, S. N., Lu, F. J., & Zou, C. L. 2018a, Science China Physics Mechanics I& Astronomy, 61, 031011
- Li, T. P., Xiong, S. L., Zhang, S. N., et al. 2018b, Sci China-Phys. Mech. Astron., 61, doi:10.1007/s11433-017-9107-5
- Li, X., Li, X., Tan, Y., et al. 2020, Journal of High Energy Astrophysics, 27, 64. <https://www.sciencedirect.com/science/article/pii/S2214404820300227>
- Li, X. F., Liu, C. Z., Chang, Z., et al. 2019, Journal of High Energy Astrophysics, 24, 6
- Li, Z. W., Liao, J. Y., Li, C. K., et al. 2017, GRB Coordinates Network, 21593, 1
- Liu, C. Z., Zhang, Y. F., Li, X. F., et al. 2020, Sci. China-Phys. Mech. Astron., 63, arXiv:1910.04955
- Luo, Q., Liao, J.-Y., Li, X.-F., et al. 2020, Journal of High Energy Astrophysics, 27, 1. <http://www.sciencedirect.com/science/article/pii/S2214404820300264>
- Preece, R. D., Briggs, M. S., Mallozzi, R. S., et al. 1998, ApJ, 506, L23. <https://doi.org/10.1086/311644>
- Sakamoto, T., Pal'Shin, V., Yamaoka, K., et al. 2011, Publications of the Astronomical Society of Japan, 63, 215
- Tierney, D., McBreen, S., Fermi Gbm Team, et al. 2010, in Eighth Integral Workshop. The Restless Gamma-ray Universe (INTEGRAL 2010), 103
- Tsujimoto, M., Guainazzi, M., Plucinsky, P. P., et al. 2011, A&A, 525, A25
- von Kienlin, A., Meegan, C. A., Paciesas, W. S., et al. 2020, ApJ, 893, 46. <https://doi.org/10.3847/1538-4357/ab7a18>
- Xiao, S., Xiong, S., Liu, C., et al. 2020, Journal of High Energy Astrophysics, 26, 58. <https://www.sciencedirect.com/science/article/pii/S2214404820300069>
- Xie, F., Zhang, J., Song, L. M., Xiong, S. L., & Guan, J. 2015, Astrophysics and Space Science, 360, 1. <http://dx.doi.org/10.1007/s10509-015-2559-1>
- Zhang, P., Wang, W., Su, Y., et al. 2021, ApJ, 918, 42
- Zhang, S., Zhang, S. N., Lu, F. J., et al. 2018, in Space Telescopes and Instrumentation 2018: Ultraviolet to Gamma Ray, ed. J.-W. A. den Herder, S. Nikzad, & K. Nakazawa, Vol. 10699, International Society for Optics and Photonics (SPIE), 434 – 455. <https://doi.org/10.1117/12.2311835>
- Zhang, S. N., Li, T. P., Lu, F. J., & et al. 2020, Sci China-Phys. Mech. Astron., 63, doi:10.1007/s11433-019-1432-6
- Zheng, Y. G., Cai, C., Du, Y. F., et al. 2020, GCN, 26815